CHEMICAL ANALYSIS OF FINE PARTICULATE MATTER MEASURED WORLDWIDE THROUGH GLOBAL AIR SAMPLING NETWORK

by

Jacob A. McNeill

Submitted in partial fulfillment of the requirements

for the degree of Master of Science

at

Dalhousie University

Halifax, Nova Scotia

April 2021

To my family and friends for their love and support –

it means more than you can ever know.

Table of Contents

LIST OF TABLES

LIST OF FIGURES

ABSTRACT

Globally consistent measurements of airborne metal concentrations in fine particulate matter (PM2.5) are important for understanding potential health impacts, prioritizing air pollution mitigation strategies, and enabling global chemical transport model development. PM2.5 filter samples (N ~ 1000 from 21 locations) were collected from a globally distributed surface particulate matter sampling network (SPARTAN) and analyzed for particulate mass and trace metals content. Metal concentrations exhibited pronounced spatial variation, primarily driven by anthropogenic activities. PM2.5 levels of lead, arsenic, chromium, and zinc were significantly enriched at some locations by factors of 100–10000 compared to crustal concentrations. Levels of metals in PM2.5 exceeded health guidelines at multiple sites. For example, Dhaka and Kanpur sites exceeded the US National Ambient Air 3-month Quality Standard for lead (150 ng/m^3). The high concentrations of several potentially harmful metals in densely populated cites worldwide motivates expanded measurements and analyses.

LIST OF ABBREVIATIONS AND SYMBOLS USED

Abbreviations

AERONET	Aerosol Robotic Network
AMS	Aerosol mass spectrometry
AOD	Aerosol optical depth
CV	Coefficient of variation
EDXRF	Energy dispersive X-ray fluorescence
EF	Enrichment factor
EPA	Environmental Protection Agency
FTIR	Fourier transform infrared spectroscopy
HIPS	Hybrid integrating plate/sphere
IARC	International Agency for Research on Cancer
IC	Ion chromatography
ICP-MS	Inductively coupled plasma mass spectrometry
IMPROVE	Interagency Monitoring of Protected Visual Environments
IUPAC	International Union of Pure and Applied Chemistry
LOD	Limit of detection
MAIA	Multi-Angle Imager for Aerosols
MAPLE	Mortality-Air Pollution Associations in Low-Exposure Environments
NAAQS	National Ambient Air Quality Standards

NASA	National Aeronautics and Space Administration
PM	Particulate matter
$PM_{2.5}$	Particulate matter with diameter under 2.5 microns (fine particulate matter)
PM_{10}	Particulate matter with diameter under 10 microns
PM_c	Particulate matter with diameter between 10-2.5 microns (coarse particulate matter)
RA	Relative abundance
RH	Relative humidity
SE	Standard error
SPARTAN	Surface Particulate Matter Network
UV-Vis	Ultraviolet-visible spectroscopy
WHO	World Health Organization
XRF	X-ray Fluorescence

Symbols

d_i	Relative percent difference
m	Slope of regression
n	Number of data pairs
r	Correlation coefficient
s	Sample standard deviation
σ	Population standard deviation
$[X]/ X_i /Y_i$	Concentration of species X/Y

ACKNOWLEDGMENTS

First and foremost, I would like to thank Dr. Randall Martin for his tireless work as my supervisor, but most importantly as a mentor and as a leader. Randall is a champion of all his students, and his positivity and versatility are truly inspirational qualities, especially considering all of the additional challenges that were piled on top of typical academic life in the past year.

I would also like to thank the whole SPARTAN team, past, present, and future, for all of the time and energy they have put into this project that I was lucky to be part of. In particular, I want to extend my thanks to: Professors Michael Brauer, Yinon Rudich, Rachel Chang, and Rajan Chakrabarty for developing and supporting SPARTAN; all of the SPARTAN collaborators (spartan-network.org) for their invaluable work; Graydon Snider, whose work paved the way for SPARTAN generally and this work specifically; Robyn Latimer for her contributions to this work; Paul Bissonnette for his many contributions to SPARTAN and the Martin lab; Xuan Liu and Chris Oxford for continuing SPARTAN operations moving forward at WashU; Crystal Weagle, whose influence on SPARTAN has been and continues to be immense and invaluable; Brenna Walsh for her tackling of logistical challenges big and small; Emmie Le Roy and especially Emily Stone for their tireless work in the SPARTAN lab, without which this thesis would have been impossible.

I would like to thank the entire Martin Lab, at both Dalhousie University and Washington University in St. Louis, for their intellectual support and friendship over the course of my time in the group. A special mention to Melanie Hammer, Yanshun Li, Jun Meng, Inderjeet Singh, Emily Stone and especially Liam Bindle - our journey from Halifax to St. Louis was an unforgettable experience that I am thrilled we got to share. The Martin group is filled with multi-talented and great people, and it was an honour to work alongside all of you.

I would also like to thank the members of the Energy, Environmental & Chemical Engineering department at Washington University in St. Louis who helped make my (unfortunately shortened) time there rewarding and exciting. I would like to additionally thank the members of the Dalhousie Graduate Chemistry Department, current and former, for all of their support, friendship, and inspiration over the years (and the Chembeers).

Finally, I would like to thank my family and friends for their love and support – without them none of this would have been possible.

1 INTRODUCTION

Some portions of this thesis are adapted from "Large Global Variations in Measured Airborne Metal Concentrations Driven by Anthropogenic Sources" by Jacob McNeill et. al, published December 2020 in Scientific Reports *(Sci Rep* ***10,*** *21817 (2020), https://doi.org/10.1038/s41598-020-78789-y), Creative Commons Attribution 4.0 International License. Jacob McNeill claims a substantial contribution of both the research and writing of said manuscript, and as such will be including work from it in this thesis in both adapted and original format. Specifically, the author made significant contributions to data analysis, experimental design, and the drafting and completion of the manuscript. A note describing this fact can be found at the end of each relevant chapter of the thesis.*

1.1 PROJECT BACKGROUND

Ambient fine particulate matter ($PM_{2.5}$, particles with diameter under 2.5 microns) has been determined to be the leading environmental risk factor for human health[1], and as such compels further study. These particles of varying chemical composition are released into the atmosphere from many sources, including combustion, industry, crustal, agriculture, and many more. Once in the atmosphere, these particles can affect the chemistry of the atmosphere, be transported to and deposited in diverse locations, and reduce air quality in affected locations. The global impact of $PM_{2.5}$ is wide-ranging, changing atmospheric

composition, damaging ecosystems, and causing adverse health effects when inhaled. The latter is of greatest concern for humans, as The Global Burden of Disease estimated that 3 million premature deaths (9% of all deaths) and 80 million years of lost healthy life were attributable to outdoor $PM_{2.5}$ on a global scale in 2017.[1]

Particulate matter has become an issue of global importance, but science and technology surrounding ambient PM lags behind what is necessary for proper assessment and understanding of the true global impact. In the sense of technology, $PM_{2.5}$ monitoring is extremely sparse in the majority of the world, with 141 of 234 countries in the world having no regular $PM_{2.5}$ monitoring over 2010-2016.[2] Research has attempted to circumvent this scarcity of data through various means, including chemical transport models, satellite estimates, and remote sensing, but these techniques cannot reliably replace real measurements worldwide due to their various limitations and biases.

A lack of measurements of $PM_{2.5}$ worldwide has also hindered the ability of researchers to fully understand how PM affects human health. Specifically, scientific understanding of the exact nature and scope of health impacts from $PM_{2.5}$ exposure is incomplete, although several strong linkages have been shown between ambient particulate matter exposure and adverse human health effects. These include cardiovascular disease[3], respiratory disease[4], cancer[5], oxidative stress[6], and type 2 diabetes.[7] The combination of serious health impacts and insufficient regular $PM_{2.5}$ monitoring invites further research, and this project aims to add to the body of literature regarding $PM_{2.5}$ measurements. In particular, this project looks to provide reliable $PM_{2.5}$ data for a variety of global sampling sites, looking specifically at the trace metal concentrations in $PM_{2.5}$ at these locations. Trace metals such as lead, arsenic,

nickel, and zinc have been shown to have negative health impacts and can be found in elevated levels in $PM_{2.5}$ at locations worldwide. This research aimed ultimately to determine the presence and concentration of various trace metals in $PM_{2.5}$ samples taken from the Surface PARTiculate mAtter Network (SPARTAN) over several years in globally disperse locations, evaluate potential sources of those metals, and assess areas that could be at risk of adverse health effects stemming from trace metal $PM_{2.5}$.

1.2 PARTICULATE MATTER ($PM_{2.5}$, PM_{10}, PM_C)

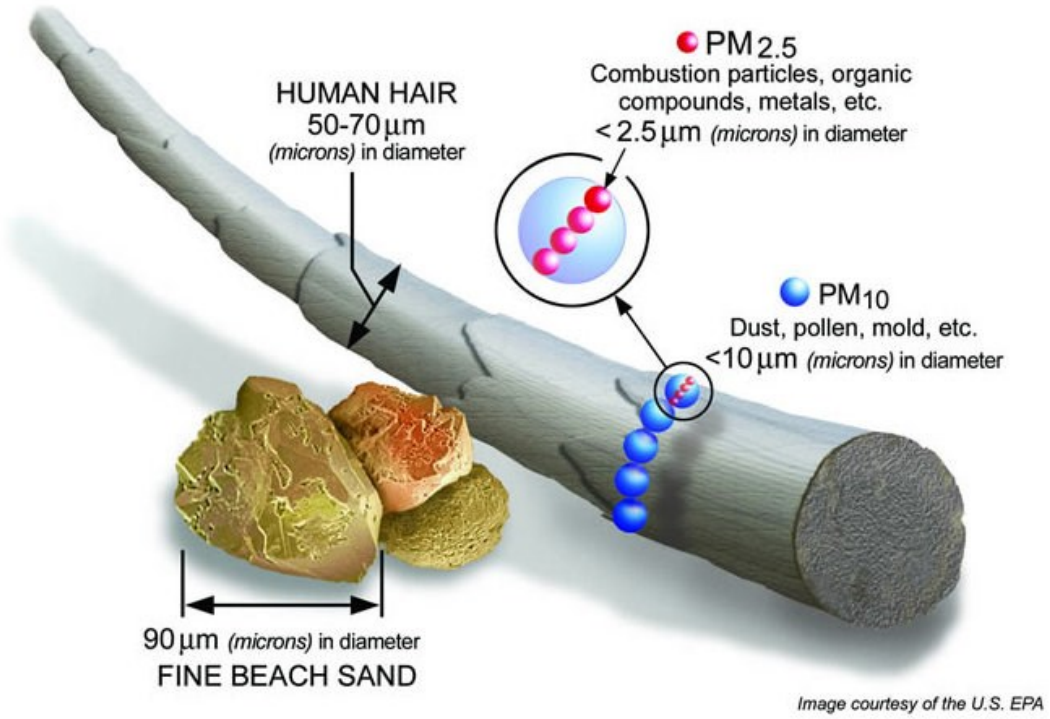

Figure 1.1: Size comparison between $PM_{2.5}$, PM_{10}, human hair, and beach sand, reproduced courtesy of the U.S. Environmental Protection Agency.[8]

Particulate matter is an area of expanding interest among atmospheric scientists, health scientists, and epidemiologists. A size comparison for particulate matter can be seen in Figure 1.1, obtained from the U.S. EPA. Three size descriptors are typically used in discussion of particulate matter: (1) fine PM (typically denoted as $PM_{2.5}$), particles in the air with a diameter under 2.5 microns; (2) PM_{10}, particulate matter with diameter under 10 microns – it should be noted that PM_{10} is inclusive of $PM_{2.5}$ by definition; (3) coarse PM (PM_c), particles with diameter ranging from 10-2.5 microns, with this size bracket used to essentially separate $PM_{2.5}$ from PM_{10} measurements. The nature of these particulates demands their understanding across a variety of fields due to their origins, behaviour, and effects. Specifically, $PM_{2.5}$ has been established as the major indicator of ambient particulate matter, and as such will be the primary focus of discussion in this work.

1.2.1 Origins of $PM_{2.5}$

Fine particulate matter can be formed through a variety of mechanisms, which are typically classified into several groups. Some of the main sources of $PM_{2.5}$ include crustal sources (resuspension of road dust, suspension of eroded particles by wind), combustion sources (burning of coal, natural gas, and gasoline for various energy needs, biomass burning such as wildfires), industrial sources (release of metal particulates through smelting and other processes), marine sources (suspended sea salt particles), and biogenic sources (organic compounds released by plants).[9] Knowledge of these sources and the chemical nature of the particulates they produce can be used to perform source apportionment of $PM_{2.5}$, which is typically done through determination of mass of various chemical markers for each

source. For example, a known mass concentration of sodium can be used to infer the mass concentration of sea salt in a given $PM_{2.5}$ sample. When a wide variety of the chemical components in the $PM_{2.5}$ sample are known, the mass concentrations stemming from different sources can be inferred through equations such as those proposed by Malm and coauthors[10]. However, ambient PM is not limited to emitted particles, as those particles can undergo chemical reactions while being transported through the atmosphere. In order to fully characterize a $PM_{2.5}$ sample, the chemical behaviour of emitted particles must also be accounted for.

1.2.2 Chemical Behaviour of $PM_{2.5}$

Once particulates are released into the atmosphere, there are a variety of reactions that can occur to create new particulates or alter existing ones. One of the most common ways that this can happen is through photochemistry, wherein volatile organic compounds (VOCs) can undergo photochemical oxidation to form a new secondary organic aerosol (SOA) compound. These SOA compounds are typically less volatile than their origin compounds and as such accumulate in the atmosphere to a greater degree. Based on the scope of the organic compounds that can be released through biogenic sources (including terpenes, xylenes, and other hydrocarbons) and the wide variety of reactions that these compounds can undergo in the atmosphere, the formation pathways for SOA are still an area of active research. Some of the methods used currently to determine organic compounds in sampled $PM_{2.5}$ include aerosol mass spectrometry [11] and Fourier-transform infrared spectroscopy [12].

Organic compounds are not the only chemically active species found in ambient $PM_{2.5}$, as there are also a variety of metals and other trace elements that can be present in fine particulate matter. These particulates can then react with the environment or organisms that breathe in $PM_{2.5}$ to cause chemical changes to the biosphere. In particular, metals such as lead, arsenic, nickel, and zinc that are released through a variety of anthropogenic sources can prove hazardous to human and environmental health if significantly present in $PM_{2.5}$.[13,14]

1.2.3 Environmental and Health Effects of $PM_{2.5}$

The environmental impacts of increasing global industrialization are widespread and well-documented across a range of disciplines, and atmospheric science is no exception. The impact of increased ambient particulate matter released from anthropogenic sources has been shown to negatively impact ecosystems in a variety of ways, and is an important side effect of high levels of ambient $PM_{2.5}$. One such mechanism is the deposition of $PM_{2.5}$ into bodies of water, which can acidify waters, increase metal concentrations, and harm aquatic life. The impact of $PM_{2.5}$ introduction into these ecosystems was demonstrated by Chinese researchers on freshwater snails, where treatments with $PM_{2.5}$, aluminum, and sulfuric acid all demonstrated negative impacts on snail behaviour.[15] Further research has observed negative impacts on fish growth from wet deposition of $PM_{2.5}$, with more deleterious effects stemming from industrial $PM_{2.5}$ deposition rich in metals compared to lower concentrations deposited from other emission sources.[16]

The environmental impact of $PM_{2.5}$ extends to flora as well as fauna, as many plants exhibit negative responses to elevated levels of ambient particulate matter. These responses can be acute (stemming from a large, short-term quantity of PM exposure) or chronic (resulting from long-term PM exposure), with both typically resulting in poor plant health, decreased photosynthesis, and reduced growth in sensitive plant species. In particular, heavy metal PM has been shown to harm vegetation through oxidative stress and disruptions to biosynthetic pathways.[17] These negative effects on vegetation can result in harmful impacts on biodiversity, agriculture, and health of organisms in the ecosystem, and are important to consider alongside the implications of $PM_{2.5}$ pollution on animal and human health.

The impacts of $PM_{2.5}$ on human health is an area of extensive study and not yet fully understood, but it is widely accepted that exposure to $PM_{2.5}$ has serious adverse effects on human health. Exposure to ambient fine particulate matter was determined to be the leading environmental risk factor for early mortality in the most recent Global Burden of Disease assessment[1], responsible for an estimated 3 million premature deaths worldwide in 2017. These premature deaths stem from a variety of $PM_{2.5}$-induced or exacerbated conditions such as cardiovascular disease[3], respiratory disease[4], cancer[5], oxidative stress[6], and type 2 diabetes[7]. The famous "Harvard Six Cities Study" firmly established the link between air pollution and mortality by studying residents of six U.S. cities with varying levels of $PM_{2.5}$ over roughly 15 years, and determining that risk factor adjusted mortality was greater for residents of cities with greater levels of ambient particulate matter.[18]

Several studies over the following decades have investigated various impacts of $PM_{2.5}$ on health conditions and their links to morbidity and mortality. In particular, increases of 10

$\mu g/m^3$ of $PM_{2.5}$ concentrations were found to increase mortality from all causes by 4%, lung cancer by 6%, and cardiovascular issues by 8%.[19] Another study found the same 10 $\mu g/m^3$ increase in ambient fine particulate matter to cause a 15-27% lung cancer mortality increase in non-smokers. Short-term increases in $PM_{2.5}$ can also result in negative health impacts, such as those proposed by a US study linking increased levels of $PM_{2.5}$ to hospitalizations from cardiovascular and respiratory issues.[20] Similar examinations of the health impacts of $PM_{2.5}$ have been carried out in Eastern countries, with one study linking up to 15.5% of total deaths in China in 2015 to ambient $PM_{2.5}$ exposure.[21] Health impacts of ambient particulate matter are critical to the safety of the global population, in particular considering that an estimated 87% of the population was living in areas exceeding the World Health Organization's air quality guideline of a maximum of 10 $\mu g/m^3$ annual average $PM_{2.5}$ in 2013.[22]

Recently, exposure to $PM_{2.5}$ has been investigated as a potential risk factor in mortality from COVID-19, the novel coronavirus strain that led to a global pandemic in early 2020. Early research out of Harvard University estimated that an increase of 1 $\mu g/m^3$ in long-term $PM_{2.5}$ exposure could result in an 11% rise in the COVID-19 death rate among Americans.[23] Long-term exposure to $PM_{2.5}$ was hypothesized to have negative impacts on the lungs through overexpression of the ACE-2 receptor, which is the cellular entry point for COVID-19, potentially leading to worse health outcomes for infected individuals with higher $PM_{2.5}$ exposure. This hypothesis was first detailed by Italian researchers who noted similar increases in mortality from COVID-19 in polluted areas of Italy compared to those with lower levels of $PM_{2.5}$.[24] This additional health impact of long-term $PM_{2.5}$ exposure

adds an extra degree of urgency to the study of ambient particulate matter, especially its relationship to human health and mortality.

1.3 SURFACE PARTICULATE MATTER NETWORK (SPARTAN)

The Surface PARTiculate mAtter Network (SPARTAN) was founded in 2012 as a collaborative grass-roots network, with the stated goal of expanding the number of available ground-level measurements of fine particulate matter ($PM_{2.5}$) through strategic placement of monitoring stations in various global areas of interest. The globally distributed surface particulate matter sampling network was designed to address the lack of reliable particulate matter measurements in densely populated regions with high pollution levels, as well as provide a link between ground-based measurements and satellite observations.

Each of the SPARTAN monitoring sites operates with the assistance of one or more collaborators located at or near the site – a full list can be found online at the SPARTAN website (www.spartan-network.org). The grassroots nature of the SPARTAN network spurs creative collaborations and links between sites across the world, and aims to provide vital and actionable information on ambient particulate matter to local, national, and international groups.

1.3.1 SPARTAN Overview

SPARTAN was designed with three major complementary components: direct air sampling to obtain speciated $PM_{2.5}$ and PM_{10} data, integrating nephelometers to provide aerosol

scattering data, and aerosol optical depth (AOD) measurements from collocated Aerosol Robotic Network (AERONET)[25] sun photometers. The combination of all three components provides a cohesive picture of the air quality at each SPARTAN site and has been used to both directly compare ground measurements to satellite observations[26], as well as interpret global chemical transport model simulations.[27]

SPARTAN site selection favours densely populated, globally dispersed regions which are underrepresented in terms of availability of representative and long-term air quality data. Local site-selection favors representative environments that avoid anomalous sources; low rooftops in urban environments are desirable to increase fetch, diminish local traffic influence, and offer instrument security. Locations of SPARTAN sites are shown in Figure 1.2, and further site information (elevation, latitude, longitude, active status) is detailed in Table 1.1. Sampling through SPARTAN has also occurred at several North American sites through various projects. Three pilot sites in the United States sampled in 2014-2016, and five sites located across Canada sampled over 2017-2019 as part of the MAPLE (Mortality-Air Pollution Associations in Low-Exposure Environments) project.[28] Over 1000 $PM_{2.5}$ filters have been analyzed as of March 2021 and were included in this study.

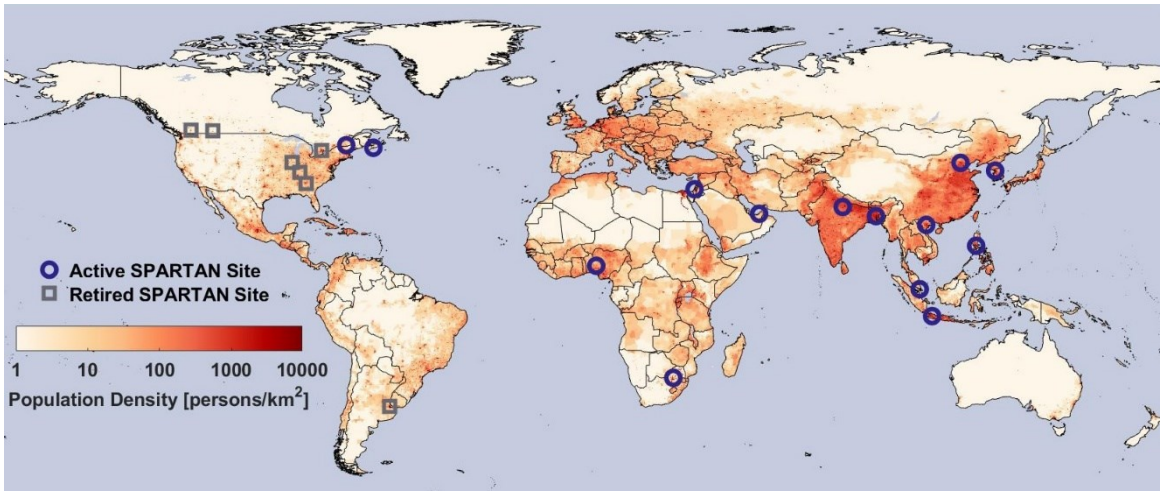

Figure 1.2: Open blue circles indicate the location of active SPARTAN sampling sites while retired sites are shown in open grey squares, overlaid on a background color map of population density (NASA SEDAC GPW [29], made using MATLAB R2019b - https://www.mathworks.com/products/matlab.html).

Table 1.1: SPARTAN site information. Sites are sorted from highest population density to lowest.

City	Country	Host Institute	Latitude	Longitude	Elevation (m)	Site type	Population density (/km^2) [a]	Active (Y/N)
Dhaka	Bangladesh	University of Dhaka	23.728	90.398	34	Megacity[b]	80790	Y
Bandung	Indonesia	Institute of Technology Bandung	-6.888	107.610	826	Urban background	22280	Y
Hanoi	Vietnam	Vietnam Academy of Science	21.048	105.800	40	Urban background	21430	Y
Manila	the Philippines	Manila Observatory	14.635	121.078	63	Megacity	20700	Y
Seoul	South Korea	Yonsei University	37.564	126.935	97	Megacity	18362	Y
Beijing	China	Tsinghua University	40.004	116.326	92	Megacity	18300	Y
Pretoria	South Africa	CSIR	-25.757	28.280	1449	Urban background	13400	Y
Buenos Aires	Argentina	CITEDEF	-34.555	-58.506	26	Megacity	9160	N
Singapore	Singapore	National University of Singapore	1.298	103.780	30	Urban background	5460	Y
Halifax	Canada	Dalhousie University	44.638	-63.594	65	Urban background	5040	Y
Toronto	Canada	Environment Canada	43.790	-79.470	186	Urban background	3800	N
Kanpur	India	IIT Kanpur	26.513	80.232	123	Urban background	3250	Y
Ilorin	Nigeria	University of Ilorin	8.484	4.675	400	Urban background	1620	Y
Rehovot	Israel	Weizmann Institute	31.907	34.811	73	Urban background	1440	Y

City	Country	Host Institute	Latitude	Longitude	Elevation (m)	Site type	Population density (/km^2)[a]	Active (Y/N)
Sherbrooke	Canada	Université de Sherbrooke	45.380	-71.931	251	Urban background	1190	Y
Lethbridge	Canada	University of Lethbridge	49.682	-112.869	904	Urban background	590	N
Atlanta	USA	Emory University	33.688	-84.290	250	Suburban	540	N
Kelowna	Canada	Environment Canada	49.941	-119.400	456	Urban background	61	N
Abu Dhabi	UAE	Masdar Institute	24.442	54.617	4	Urban background	31	Y
Mammoth Cave	USA	Mammoth Cave National Park	37.132	-86.148	235	Natural	13	N
Bondville	USA	University of Illinois	40.053	-88.372	200	Rural	2	N

[a]Population density is reported for a 1 km radius based on NASA's Gridded Population of the World.[29]
[b]Megacities are defined as having 10 million or more inhabitants.[30]

1.3.2 SPARTAN Sampling Procedure

In order to assure consistency across all SPARTAN sites, network-wide procedures for sampling were developed to achieve the main goals of the network: measurement of long-term ambient PM concentrations at various global locations, obtained in a cost-effective and operator-friendly way. To summarize the overall procedure, when a new SPARTAN site is selected, the site operator(s) are shipped instrumentation (all to this date manufactured by AirPhoton, LLC) that is installed on location, as well as filter cartridges for PM sampling. Once instrument and cartridge are installed and the sampling is initiated, the instrument runs near-autonomously until the cartridge sampling period completes, at which point the operator collects the sampled cartridge and ships it to the SPARTAN laboratory for analysis, and installs the next cartridge to begin another sampling period.

In the original procedure, PM_c and $PM_{2.5}$ filter masses were collected on a two-stage stacked filter unit inside rooftop-mounted AirPhoton SS4i automated air samplers over nine-day periods. A removable filter cartridge protected seven sequentially active pairs of coarse Nuclepore and fine Teflon filters, plus a pair of travelling blanks. Beginning in late 2017, sampling stations at SPARTAN were upgraded to the AirPhoton SS5 models, which use a cyclone inlet to separate particles by varying flow rates (5 and 1.5 liters per minute, respectively, for $PM_{2.5}$ and PM_{10} size-cuts) through the station. This allowed for elimination of the Nuclepore filters and the introduction of filter cartridges with eight total stretched Teflon filters which included six sampling $PM_{2.5}$, one sampling PM_{10}, and one travelling blank. These cartridges were pre-assembled in the SPARTAN central laboratories at Dalhousie University, and shipped to sites for installation by site operators. Once the filter cartridges are installed, the sampling stations run autonomously for the cartridge duration. For international sites, each of the $PM_{2.5}$ filters are sampled for rotating 3-hour spans over nine days, totaling 24 hours of sampling. Taking this information across the entire diurnal cycle over a 9-day period, rather than sampling for 24 hours straight, helps to better capture long-term averages.[31] A sampling period for one $PM_{2.5}$ filter (at an international site) is shown in Figure 1.3.

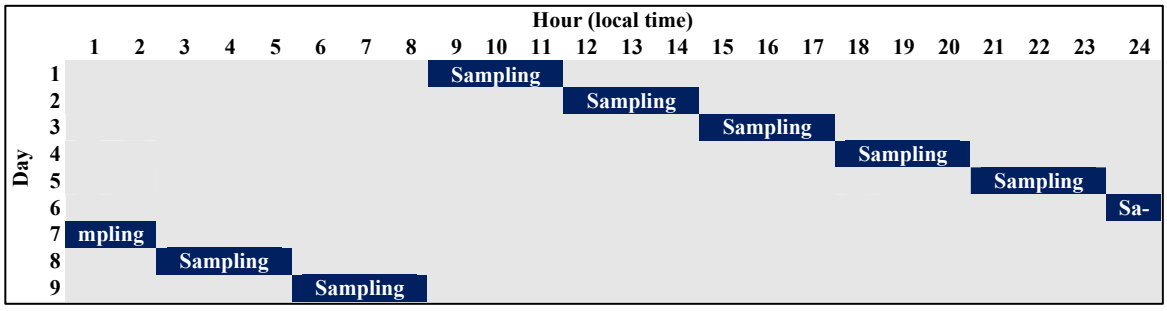

Figure 1.3: Sampling period for a typical SPARTAN $PM_{2.5}$ filter at an international site.

The PM_{10} filter is sampled for a 30-minute period after each 3-hour $PM_{2.5}$ sample for the entire 54-day sampling period, providing a 54-day average PM_{10} concentration. For sites which were part of the MAPLE cohort, each filter samples for a total of 48 hours (6-hour periods for the $PM_{2.5}$ filters and 1-hour periods for the PM_{10} filters) to ensure a quantifiable amount is deposited in these low-PM environments. Once sampling was complete, filter cartridges were removed from the sampling station, sealed, and returned to the central laboratory at Dalhousie University for chemical and physical analysis of the filters. Filters were analyzed to determine $PM_{2.5}$ or PM_{10} mass (gravimetric), water-soluble ions (ion chromatography with conductivity detection), black carbon (absorbance, determined through smoke-stain refractometry), and trace metals (inductively coupled plasma mass spectrometry and later X-ray fluorescence analysis). Further details on lab analysis for SPARTAN filters are discussed in Chapter 2.

1.4 Inductively Coupled Plasma Mass Spectrometry (ICP-MS)

Inductively coupled plasma mass spectrometry (ICP-MS) is a multi-element analysis technique used extensively in various disciplines including geology[32], cell biology[33], and food science[34]. The multi-element aspect of ICP-MS analysis is advantageous in comparison to other methods previously or concurrently used for single-element analysis such as atomic absorption analysis, which require individual set-ups for each element of interest. This elemental versatility stems from the use of electrically generated plasma (typically argon) used to ionize samples (which have been nebulized before introduction into the system) in order for the ions to be sent to the mass spectrometer to be quantified.

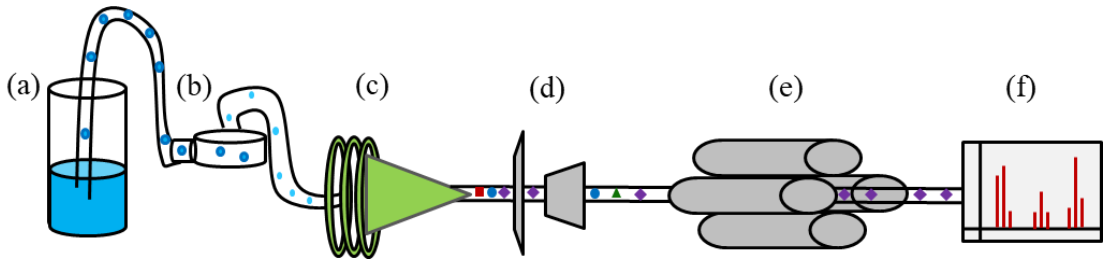

Figure 1.4: Simplified schematic diagram of an inductively coupled plasma mass spectrometer (ICP-MS): (a) samples are prepped and digested, sent to (b) spray chamber for nebulization before entering (c) ICP torch, with argon plasma ionizing and atomizing sample. Ions (shown in various colour/shape patterns) pass through (d) interface of sample and skimmer cones before mass-dependent separation by (e) quadrupole mass analyzer prior to (f) detection of ions of interest by instrument detector.

This process can be broken down into general steps as seen in Figure 1.4: a) sample prep, wherein samples are made into solution, typically through addition of deionized water, a small quantity of acid, and then digested; b) nebulization of the solution and introduction of the aerosol into the inductively coupled plasma torch; c) ionization and atomization of the sample by the argon plasma; d) transmission of some of the generated ions through the "interface" (a set of metal cones); e) mass-based separation of the transmitted ions through various methods, most commonly a quadrupole mass analyzer; f) detection of the separated ions at the instrument detector.[35] Upon completion of the sample analysis, the mass spectrum for the sample will be output, which can be used in concert with reference standards and/or isotopic labelling in order to determine elemental concentrations in the original solution.

It should be noted that ICP-MS analysis has limitations that can have a notable impact on results for certain elements. In particular, proper digestion of the sample is key to ensuring accurate elemental quantification, and in practice this can be difficult to achieve. Fully

digesting samples with a number of different crustal elements can be notably tough, as nitric acid extraction efficiencies for some crustal elements such as Al and Fe can be as low as 50%.[36] Digestion can be performed with stronger acids (including aqua regia on its own or in concert with hydrofluoric acid) with the goal of higher recoveries for such elements, but these acids can cause spectral interferences and are more hazardous to operators, especially hydrofluoric acid.[37] Another important aspect when considering ICP-MS analysis is that it is destructive, which can pose issues if samples are limited and further analysis is required. Despite these limitations, ICP-MS elemental analysis is still an extremely useful tool for quantification of trace elements in solid samples.

ICP-MS analysis has been used extensively for quantification of trace elements in samples of varying natures, particularly in determining trace metals. There are numerous examples of the technique in use for quantifying ambient particulate matter sampled on air filters[38–40], since as previously discussed trace metal $PM_{2.5}$ can be impactful on human health. These trace metals are also useful indicators for various particulate matter sources, and quantifying their presence can help better understand and track emissions. In collaboration with Dr. Graham Gagnon and the Centre for Water Resource Studies at Dalhousie University, ICP-MS analysis was adopted into the SPARTAN sample analysis procedure from the beginning of the network, and continued until lab operations moved from Dalhousie University to Washington University in St. Louis in 2019. Further information on the ICP-MS methods used for SPARTAN can be found in Chapter 2.

1.5 X-RAY FLUORESCENCE (XRF)

X-ray fluorescence analysis is a non-destructive elemental analysis technique used with samples of wide-ranging natures, including solids, liquids, and filters. The technique is named for the X-ray fluorescence phenomenon by which it functions, wherein X-ray photons that strike a sample result in characteristic fluorescence that can be measured directly.

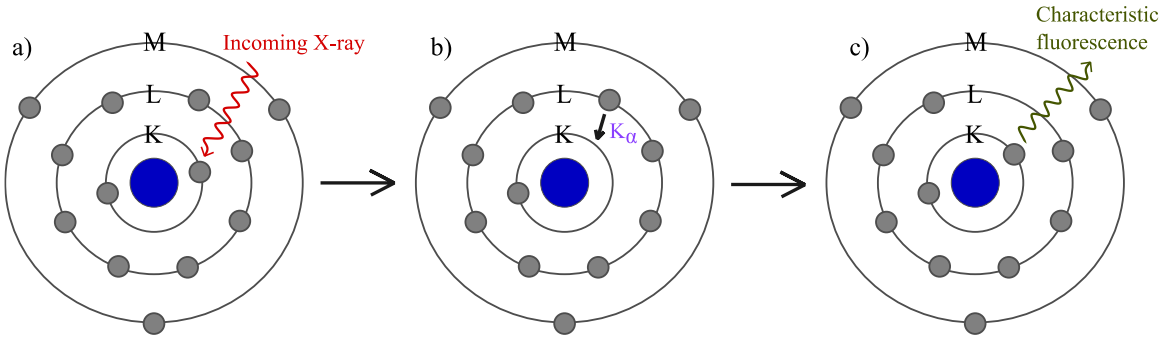

Figure 1.5: Atomic representation of mechanisms of X-ray fluorescence, where the nucleus of the atom (aluminum in this example) is shown in blue, electrons in grey, X-ray photons in red, and fluorescence in green. Shells are denoted in X-ray notation, where K is equivalent to shell 1, L to shell 2, M to shell 3, etc.

X-ray fluorescence occurs at the atomic level through a multistep mechanism shown in Figure 1.5: a) an incoming X-ray photon knocks out an electron in an atomic shell (termed initial vacancy); b) an electron from a higher atomic shell moves in to fill the vacancy; c) the excess energy from the transition is released as a characteristic photon with energy dependent on the element and transition. In XRF analysis, the characteristic photons released as fluorescence can be detected and quantified in order to create an elemental "fingerprint" – i.e. a quantification of the elemental concentrations present in the sample.

In order to achieve X-ray fluorescence, the energy of the incoming X-ray photon must be close in energy to the specific energy of the elemental transition in question.

1.5.1 X-ray Notation

XRF applications typically describe these electronic transitions by use of X-ray notation, where the electron shells are represented by K (1*s*), L (2*s*, 2*p*), M (3*s*, 3*p*, 3*d*), and so on. Using this notation, transitions can be represented in one of two ways: traditional Siegbahn notation, or the newer IUPAC nomenclature. An example of Siegbahn notation would be Kα, where K represents the final shell after the transition, and α represents the starting point of the transition, in this case the L shell. This notation can be further specified through an additional digit at the end (i.e. $K\alpha_1$) which is unique to a particular L subshell (here L_3 or $2p_{3/2}$), but not necessarily the same as the digit of the L subshell. Due to the somewhat confusing nature of this nomenclature, IUPAC has developed a newer notation that simply takes the final shell of the transition and combines it with the initial subshell of the transition.[41] For example, a $K\alpha_1$ transition would be represented as K-L_3, as the electron from the L_3 subshell moves into the K shell. A partial summary of the transitions and their notation can be found in Table 1.2 – note that many other transitions are possible but are less commonly used and will not be discussed in this work.

Each transition has its own unique energy that is a product of both the element in question that is being excited by X-rays, as well as the specific transition that occurs. Photons released during this transition have the excess energy between the initial and final electronic states, which is characteristic of both element and transition. When measured, these

transitions are typically referred to by their final state – i.e. K-lines, L-lines, etc. Since the energy difference between some transitions is very small, measurements may be combined in software; for example, a Kα measurement may include both the $K\alpha_1$ and $K\alpha_2$ lines if spectral resolution is not high enough to separate the two peaks.

Table 1.2: Partial listing of common electronic transitions used in X-ray fluorescence analysis, as well as their notations in both Siegbahn and IUPAC notation.

Final state	Initial state	Siegbahn	IUPAC
K (1*s*)	L_2 ($2p_{1/2}$)	$K\alpha_2$	$K\text{-}L_2$
	L_3 ($2p_{3/2}$)	$K\alpha_1$	$K\text{-}L_3$
	M_2 ($3p_{1/2}$)	$K\beta_3$	$K\text{-}M_2$
	M_3 ($3p_{3/2}$)	$K\beta_1$	$K\text{-}M_3$
L_3 ($2p_{3/2}$)	M_4 ($3d_{3/2}$)	$L\alpha_2$	$L_3\text{-}M_4$
	M_5 ($3d_{5/2}$)	$L\alpha_1$	$L_3\text{-}M_5$

Typically, the strongest fluorescence is observed from K-lines, then L-lines, and so on. In order to maximize the signal-to-noise ratio, the strongest signals within the detection range are chosen, typically the Kα line(s). As atomic number increases so too does the energy of the emitted lines – this can result in heavier elements having K-lines with energies that are out of the detection ranges of common benchtop XRF analyzers. In these cases, the L-lines can then be used, or even M-lines.

1.5.2 XRF Analysis

X-ray fluorescence analysis relies on the characteristic energies released from electronic transitions in order to quantify the content of various elements or compounds in samples non-destructively. The energy of incoming radiation into the sample determines which element(s) will be subjected to analysis, as that energy must be sufficiently close to the particular electronic transition for the element. By varying the energy of the X-rays that are beamed at the sample, the characteristic transitions for a wide selection of elements can be induced and quantified. The resulting fluorescence from these transitions also varies in quantity depending on the atomic weight of the element in question, as seen in Figure 1.6.

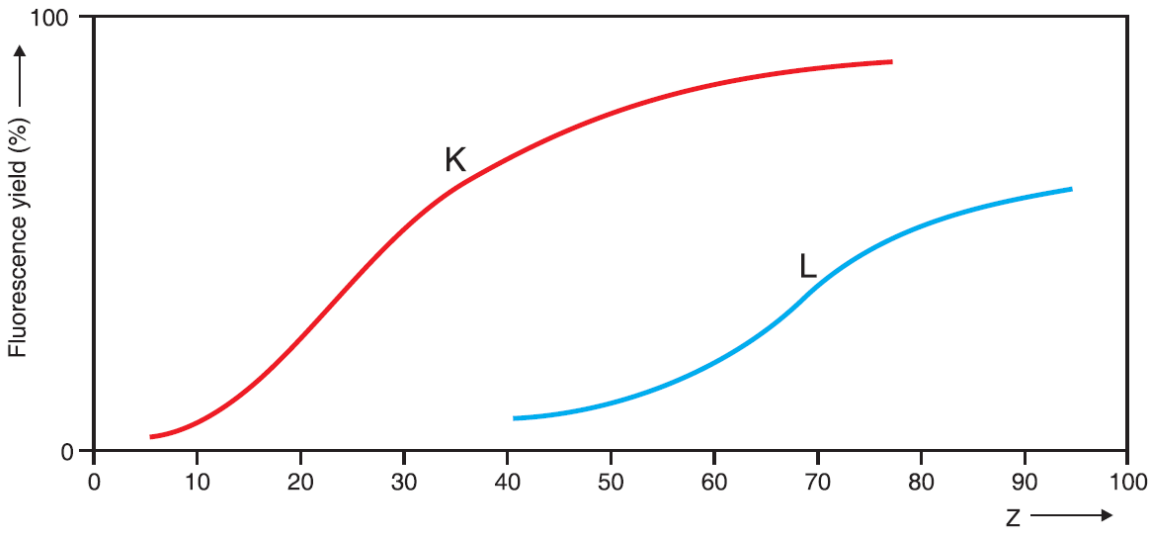

Figure 1.6: Fluorescence yield (%) as determined by atomic weight of element of interest for K- and L-transitions in XRF analysis, reproduced here from Panalytical.[42]

The quantification used to determine the variation in resulting fluorescence is fluorescence yield, described in Eq. 1.1.

$$\text{Fluorescence yield (\%)} = \frac{\text{\# of fluorescent photons released}}{\text{\# of initial vacancies (max photons)}} * 100 \qquad \text{Eq. 1.1}$$

From Figure 1.6, it can be seen that elements with lower Z numbers (i.e. lower in atomic weight) will generally result in less emitted fluorescence than their counterparts with higher Z numbers (i.e. higher in atomic weight), for both K- and L-lines. It also is apparent that using the L-transitions in XRF is more viable for heavier elements than lighter ones, and that very light elements (roughly $Z < 10$) are some of the most difficult to quantify based on their low fluorescence yield.

In practical operation, XRF analyzers use an X-ray tube with variable voltage and current to vary the energy and quantity of X-rays that are beamed at the sample in order to capture elements of interest. Emitted photons are quantified by a detector, which converts the photons into a proportionate electrical signal for the instrument to record and display. Further information on the specific conditions used for XRF analysis in this work can be found in Chapter 4.

The nature of XRF analysis provides some inherent advantages over other techniques for trace element quantification such as ICP-MS – in particular, the non-destructive nature of XRF analysis allows for repeat measurements as well as conservation of sample for other types of analysis. Using XRF compared to ICP-MS also removes the potential issue of incomplete digestion of certain metal oxides and other compounds, as XRF relies on the presence of specific atoms, versus specific ions for ICP-MS. Theoretically, this should allow for complete characterization of all atomic concentrations in samples through XRF, but in practice some issues can arise to complicate characterizations.

X-ray fluorescence is a surface technique, meaning that samples must not have varying composition throughout the thickness of the sample – in this work, this concern is mitigated by the nature of the sample deposition on air filters, which are very thin. Another potential issue stems from detection of fluorescence from the sample, as both secondary fluorescence and peak overlapping can occur. Secondary fluorescence takes place when the fluorescence released from the initial X-ray excitation strikes another atom in the sample, causing it to release fluorescence, masking the presence of the first element while exaggerating the presence of the second. Peak overlapping occurs when there are significant concentrations of a particular element(s), which results in a larger peak that may augment or mask another elemental peak. An example of this is sulfur interference, which has been shown to mask the presence of aluminum and inflate the concentration of silicon when sulfur is present in large concentrations.[43]

It is important to note that these drawbacks are present, but their impact on analysis can be accounted for and corrected in most cases, and are more minor for this work than issues with digestion and repeatability for ICP-MS and other destructive analyses. In light of its advantages, XRF analysis was implemented into SPARTAN procedures and effectively replaced ICP-MS analysis for trace element quantification in globally sampled $PM_{2.5}$.

1.6 Figures of Merit

The previously outlined methods offer an abundance of different results, but it is critical to put them into proper context for better understanding. There are some key figures of merit

used within this work to properly present and discuss the results observed at SPARTAN sampling locations around the world. These figures of merit include limits of detection, standard error, and others.

The limit of detection (LOD) is a quantification used to establish a lower limit for a measured concentration, based on the observed variance in instrument response. This limit is typically calculated as:

$$LOD = 3 * s \quad \text{Eq. 1.2}$$

where *s* is the measured standard deviation of independent blank sample measurements (typically 8-10). In practical terms, the LOD is used to account for instrument noise using the 3σ rule, wherein ~99% of normally distributed values are found within three standard deviations of the mean value, and has been shown to correspond to a confidence level of ~90%.[97] LODs are used in this work to establish the lowest reported ICP-MS and XRF measured concentrations of elements observed at SPARTAN sites.

Another metric used here to add context to reported results is the sample standard error, (SE) which is defined as such:

$$SE = \frac{s}{\sqrt{n}} \quad \text{Eq. 1.3}$$

where the standard deviation of the samples *s* is used along with the number of samples *n*. This indicator is an estimate of the degree to which the sampling mean is different from the population mean. In practical terms for this application, the SE is used to indicate how close

the mean $PM_{2.5}$ values reported for SPARTAN locations are to the true average $PM_{2.5}$ values for those locations, giving context to what the typical conditions might be in those areas. These typical values can be used to give an indication of air quality and presence of potentially harmful elements in ambient air sampled at SPARTAN sites.

1.7 PROJECT MOTIVATIONS

Many regions of the world far exceed the World Health Organization (WHO) air quality guidelines for ambient air pollution, especially for fine particulate matter ($PM_{2.5}$)[44,45], and the impact on health is substantial.[46] Nonetheless, ground-based monitoring of $PM_{2.5}$ mass concentration is inadequate for exposure assessment[2], and the select studies of $PM_{2.5}$ chemical composition measurements[47,48] are even sparser. In some locations, the majority of metal concentration measurements made to date have been of the PM_{10} fraction.[49–51] Global observations of $PM_{2.5}$ mass concentration and composition can inform aerosol model development and exposure assessment, improve understanding of emission sources and help prioritize mitigation policies [52] to reduce health impacts.

The relationship between $PM_{2.5}$ and human health[22,53] including the association of $PM_{2.5}$ with cardiovascular disease[3], respiratory disease[4], cancer[5], oxidative stress[6], and type 2 diabetes[7] has become better understood over the last few decades. However, more data are needed before effects of particular components (specifically trace metals) are well understood at a global scale. There is evidence that the oxidative potential of $PM_{2.5}$ is related to its metal content[47] as increased abundance of redox-active elements may induce

oxidative stress.[54–57] Many metals have known health effects, such as As, Cd, and Cr, which are classified by the WHO's International Agency for Research on Cancer (IARC) as known human carcinogens (IARC Group 1)[58], and Pb, which is associated with impaired cognitive function.[59] Increased cardiovascular disease rates have been associated with enhanced relative concentrations of K, Al, Ni, Zn and V[3,60] and mortality risks have been associated with preferential bioaccumulation of heavy metals such as As, Pb, and Al.[61] Various metal compounds are classified by the EPA as Hazardous Air Pollutants, including As, Cd, Co, Cr, Pb, Mn, Ni, and Se compounds. Measurements of $PM_{2.5}$ composition are needed to assess the global distribution of these deleterious metals in fine particulate matter, as they could pose significant health risks to populations living in areas of high $PM_{2.5}$ pollution.

Ground-based elemental composition can also provide information about airborne $PM_{2.5}$ burden and sources. For example, K has associations with wood burning[62–64], Zn can be linked with traffic through tire wear[65], and V derives mainly from heavy fuel oil combustion such as from shipping.[66,67] Coal is a source of multiple toxic elements such as Pb, Cr, Mn, As, and Se[66,68] whereas non-ferrous metal production is a large source of As, Cd, and Zn.[66] Vehicle traffic contributes a mix of elements including the heavy metals Ba, Zn, and Pb, as well as the crustal components Fe, Al, Mg, and Ti. [62,69]Additional observations are needed to better understand particulate matter sources and loadings, to evaluate emerging emission inventories and chemical transport models on a global scale[70,71] and to understand local and regional impacts of emission sources. To our knowledge, no other global network has measured the trace metal concentrations in $PM_{2.5}$.

The ground-based Surface PARTiculate mAtter Network (SPARTAN) is building up a long-term data set measuring PM concentration at globally distributed sites[31] and provides new data to evaluate PM composition. In this study, the trace metal composition of $PM_{2.5}$ was investigated, supplemented by coarse PM (PM_c) and PM_{10} data, in ambient air samples from SPARTAN sites around the world.

**Note: some material for this Chapter has been adapted from "Large Global Variations in Measured Airborne Metal Concentrations Driven by Anthropogenic Sources" by Jacob McNeill et. al, published in* Scientific Reports *(December 2020)*

2 METHODS

2.1 FILTER ANALYSIS PROCEDURE

The analysis of SPARTAN filters in this project was a multistep process that occurred over two distinct time periods, and in multiple locations. For both time periods, the general protocol of analysis of SPARTAN samples remained the same, but some specifics changed. The first section of analysis occurred at Dalhousie University from the beginning of the SPARTAN network until late 2019, and includes all data relating to ICP-MS. This analysis data is detailed and discussed primarily in Chapter 3. The second section of analysis occurred at Washington University from late 2019 onward, and includes all data relating to XRF. Data from this time period is examined primarily in Chapter 4.

2.1.1 Filter Analysis – Dalhousie University

The analysis procedure for filters at Dalhousie University is shown in Figure 2.1. Generally, all filters (25mm PTFE, Measurement Technology Laboratories for all $PM_{2.5}$ filters) were pre-weighed in a SPARTAN laboratory using gravimetric analysis – at Dalhousie, this was done manually using a Sartorius Ultra-Fine Balance (± 0.1 μg) in an ISO-4 clean room (20-30°C, 30-40% relative humidity (RH)). Afterwards, filters were loaded into cartridges, sent to operators at SPARTAN sites, and sampled in sampling stations as detailed in Subsection

1.3.2. Once filters were returned from the field, they were post-weighed in the same manner as the pre-weighing step.

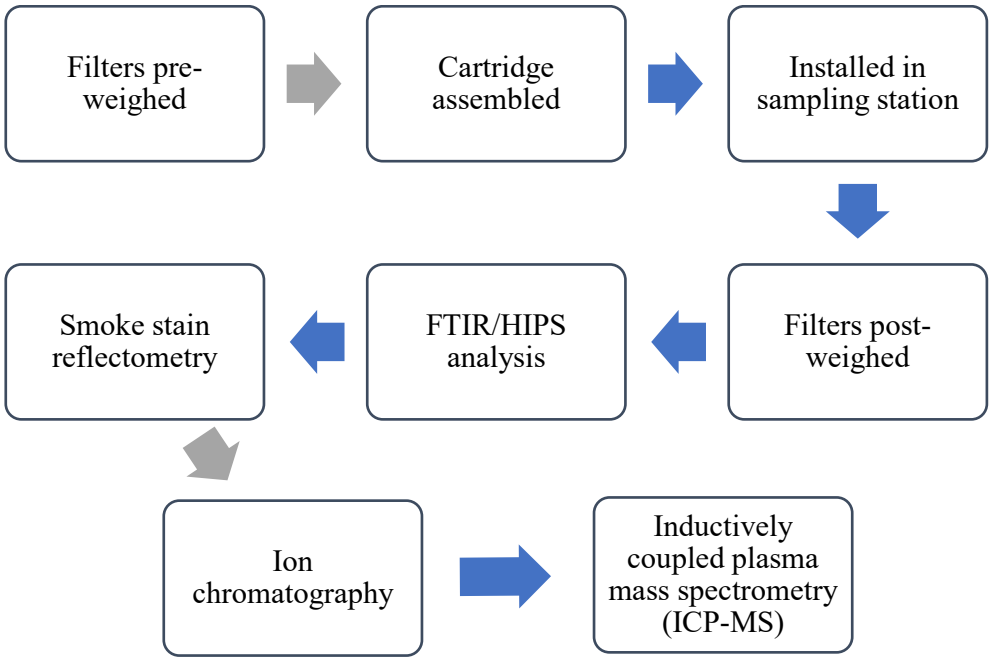

Figure 2.1: Workflow of filter analysis in the previous SPARTAN network protocol at Dalhousie University. Steps with blue arrows denote physical transfer of filters (shipping, lab transfers) while steps with grey arrows indicate filters remaining in the SPARTAN laboratory.

Once filters were post-weighed, they were then sent to collaborators at University of California, Davis for Fourier Transform Infrared spectroscopy (FTIR) and hybrid integrating plate/sphere (HIPS) analysis to obtain information on organic carbon/elemental carbon and black carbon, respectively. Upon return, filters were then analyzed by smoke stain reflectometry (EEL43M, Diffusion Systems Ltd.) to obtain effective black carbon. At this point, all filter samples were then extracted for ion chromatography analysis (IC,

Thermo Fisher Scientific Dionex Aquion) with methanol and deionized water. Two aliquots of the extract were then individually used to measure anions and cations.

Afterwards, filters at Dalhousie University were characterized through inductively coupled plasma mass spectrometry (ICP-MS, Thermo Scientific X-Series 2, Centre for Water Resource Studies at Dalhousie University), and the quantified elemental concentrations were used for the analysis detailed in Chapter 3. For each SPARTAN filter a small quantity of isopropyl alcohol (previously 30 μL, updated to 10 μL) was added, then the filter was extracted (97°C for 2 hours) with 5% trace metal grade nitric acid solution in a process similar to Fang et al.[55] and Herner et al.[72] Filters were boiled in the acidic solution and the liquid extract submitted for quantitative analysis via ICP-MS, using 25 – 500 ppb (μg/l) trace metals standards and three reference elements for atomic mass (^{45}Sc, ^{115}In, and ^{159}Tb) for each analysis. Measured concentrations from the field blank filters for each filter cartridge were subtracted from the seven corresponding samples of each cartridge to account for variable trace metal baselines. Consistent ICP-MS analysis in the central Dalhousie laboratory facilitated consistency of results across sites. It is established that nitric acid extraction efficiencies for some crustal elements such as Al and Fe can be as low as 50%[36] as discussed previously – this analysis offers perspective on this emerging dataset, with observed variability that far exceeds the factor of 2-3 uncertainty associated with some extraction efficiencies.

In order to compare SPARTAN trace metal ICP-MS measurements with independent concurrent measurements, a joint sampling campaign was conducted in the US in concert

with the IMPROVE (Interagency Monitoring of Protected Visual Environments) network. Table 2.1 details this comparison, where rows show results from the three sampling campaigns versus standardized instrumentation and sampling techniques from Atlanta[73], Bondville[74] and Mammoth Cave.[74] Excellent agreement was apparent at both Atlanta (m = 1.05 ± 0.16, r = 0.95) and Mammoth Cave (m = 1.01 ± 0.17, r = 0.94). Trace metals in Bondville were closer to SPARTAN detection limits, which may explain the slightly larger difference in concentrations there.

Table 2.1: Correlations and slopes (axis-free regression) of SPARTAN $PM_{2.5}$ versus collocated studies conducted by EPA's IMPROVE network. Elements included are those consistently above SPARTAN limits of detection.

Site	Size fraction	Number of species co-measured	Collocated sampling, log-log plot Slope ± 1σ-error	*r*	Reference Study
Atlanta	$PM_{2.5}$	22	1.05 ± 0.16	0.95	[75]
Bondville	$PM_{2.5}$	20	0.90 ± 0.21	0.88	[74]
Mammoth Cave	$PM_{2.5}$	22	1.01 ± 0.17	0.94	[74]
3 USA sites merged	$PM_{2.5}$	23	0.99 ± 0.12	0.92	EPA + IMPROVE

2.1.2 Filter Analysis – Washington University in St. Louis

The analysis procedure for filters at Washington University in St. Louis is shown in Figure 2.2. As in the previous iteration of the analysis procedure, all filters were pre-weighed in a SPARTAN laboratory using gravimetric analysis prior to field use. At Washington University, filters were weighed automatically using an automated filter weighing system (AH500E, Measurement Technology Laboratories, ± 1 μg) in an environment-controlled room (21-23°C, 38-40% RH). Afterwards, filters were loaded into cartridges, sent to

operators at SPARTAN sites, and sampled in sampling stations as detailed in Subsection 1.3.2. Once filters were returned from the field, they were post-weighed in the same manner as the pre-weighing step.

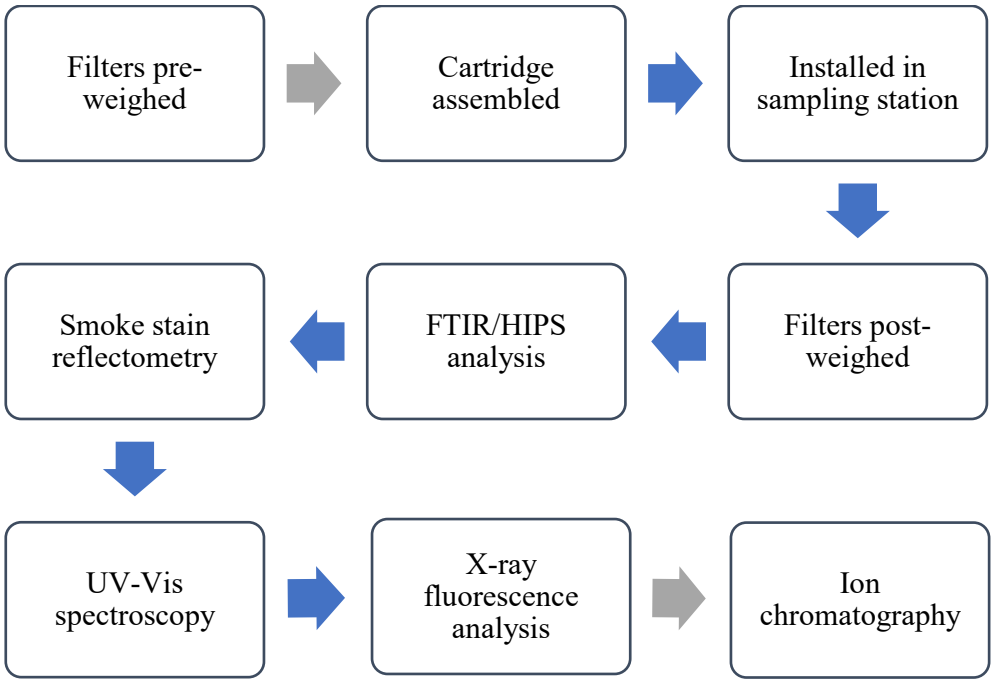

Figure 2.2: Workflow of filter analysis in the current SPARTAN network protocol. Steps with blue arrows denote physical transfer of filters (shipping, lab transfers) while steps with grey arrows indicate filters remaining in the SPARTAN laboratory.

Once filters were post-weighed, they were then sent to collaborators at University of California, Davis for Fourier Transform Infrared spectroscopy (FTIR) and hybrid integrating plate/sphere (HIPS) analysis to obtain information on organic carbon/elemental carbon and black carbon, respectively. Upon return, filters were then analyzed by smoke stain reflectometry (EEL43M, Diffusion Systems Ltd.) to obtain effective black carbon.

For filters at Washington University, the next analysis step was UV-Vis analysis, where filters were transferred to Dr. Rajan Chakrabarty's lab to quantify brown carbon. Upon completion of this step, SPARTAN filters were analyzed with X-ray fluorescence (XRF, Malvern Panalytical Epsilon 4) for trace metal quantification in lieu of ICP-MS. The non-destructive nature of XRF and improved quantification of crustal elements such as Al and Fe motivated the switch of methods. The Epsilon 4 instrument was calibrated for elements of interest using quantitatively loaded 47mm filters obtained from the University of California, Davis' Air Quality Research Center, thin-film standards from Micromatter Technologies, and the National Institute of Standards and Technology's Standard Reference Material 2783. Further information on the XRF analysis procedure is detailed in Chapter 4.

At this point, all filter samples were then extracted for ion chromatography analysis (IC, Thermo Fisher Scientific Dionex Integrion) with methanol and deionized water. Two aliquots of the extract were then individually used to measure anions and cations. Future implementation of aerosol mass spectrometry (AMS) is planned for SPARTAN analysis of organic components of particulate matter, but was not used in this work.

2.2 CRUSTAL ENRICHMENT FACTORS (EFS)

Crustal enrichment factors (EFs) were used to distinguish naturally occurring crustal elements from those released by anthropogenic sources. We compared filter-extracted elemental concentrations X to background continental concentrations from Taylor and

McLennan (1995), normalized by measured crustal Fe concentrations, which is predominantly from natural sources (e.g. Hsu et al., 2010) as seen in Eq. 2.1.

$$EF_{X,Y} = \frac{[X/Fe]_{\mathrm{PM2.5}}}{[X/Fe]_{\mathrm{Taylor}}} \qquad \text{Eq. 2.1}$$

Although natural variability in the Fe fraction in soil will affect these results, the Fe fraction in soil tends to be quite consistent.[78] Anthropogenic sources of Fe imply that the resultant enhancement ratios will be a conservative indicator of anthropogenic contribution. Nonetheless, to ensure that conclusions are not affected by using Fe as the reference element due to extraction efficiency as previously mentioned, a complementary analysis was performed by replacing site Fe concentrations with corresponding coarse PM concentrations, seen in Eq. 2.2. Coarse particulate matter over land has been established as predominantly stemming from suspended dust[10,79] (with other potential sources including urban dust and organic material), making it a suitable measure of crustal source abundance to verify the validity of results using Fe. An estimate of the concentrations of the metal oxides present in coarse PM was obtained by use of the soil reconstruction equation described by Malm and coauthors [80] and shown in Eq. 2.3, in combination with continental concentrations from Taylor and McLennan.

$$EF_{X,Y} = \frac{\left[X/_{PM_c}\right]_{\mathrm{PM_{2.5}}}}{\left[X/_{PMc^*}\right]_{\mathrm{Taylor}}} \quad \text{Eq. 2.2}$$

$$\mathrm{PM_c^*} = 2.20[\mathrm{Al}] + 2.49[\mathrm{Si}] + 1.63[\mathrm{Ca}] + 2.42[\mathrm{Fe}] + 1.94[\mathrm{Ti}] \quad \text{Eq. 2.3}$$

2.3 WHOLE SYSTEM UNCERTAINTIES

Whole system uncertainties for the SPARTAN network are estimated through use of collocated filter sampling stations. The process is described in previous work by the SPARTAN team[27] but in summary, three sites in typically low (Halifax, Canada), moderate (Toronto, Canada), and high (Beijing, China) PM environments performed collocated sampling over three week periods. Over this period, each station recorded 24-hour samples (48-hour in Halifax to ensure adequate loading) which were then analyzed as per SPARTAN protocol. This allows for a comprehensive evaluation of uncertainties across the network, as the sampling and analysis processes are duplicated for each sample in the collocated pair, but this approach may not account for systematic errors in analysis techniques. The uncertainty calculation is based on the US Code of Federal Regulations, Part 58 (Ambient Air Quality Surveillance), Appendix A, Section 4.2. For each collocated data pair, the relative percent difference, di, is calculated using Eq. 2.4:

$$d_i = \frac{X_i - Y_i}{(X_i + Y_i)^2} * 100 \quad \text{Eq. 2.4}$$

where Xi and Yi are the species concentrations from the two sampling stations. The coefficient of variation upper bound is then calculated using Eq. 2.5:

$$\mathrm{CV(upper\ bound)} = \sqrt{\frac{n*\sum_{i=1}^{n} d_i^2 - \left(\sum_{i=1}^{n} d_i\right)^2}{2n(n+1)}} * \sqrt{\frac{n-1}{\chi^2_{0.1,n-1}}} \qquad \text{Eq. 2.5}$$

where n is the number of data pairs, and $\chi^2_{0.1,n-1}$ is the upper 10th percentile of a chi-squared distribution with n – 1 degrees of freedom. The factor of 2 in the denominator adjusts for the error in d_i from two measurements. These CV values (or uncertainties) indicate the potential of variability in reported ICP-MS results for each of the elements in question through the SPARTAN methodology. Other factors that can influence the variations of observed concentrations are site-specific factors like wind, local emissions, and temporality of sampling – these reported uncertainties are independent of those factors by nature of the collocation. These uncertainties are not applicable to XRF-measured results – this is further discussed in Chapter 5.

Whole system uncertainties for the trace metals analyzed during this collocation are shown in Table 2.2, with both site-specific values as well as values for the whole SPARTAN network. Network-average values were lowest for $PM_{2.5}$ (14.7%), Pb (15.4%), P (16.9%), and Fe (16.9%). Plots for individual components are shown in Figure 2.3.

Table 2.2: Uncertainties (%) as calculated through Eq. 2.5 for $PM_{2.5}$ and trace metals quantified by ICP-MS during collocated sampling.

Location	# of filters	PM2.5	As	Co	Cr	Cu	Fe	Li	Mg	Mn	Na	P	Pb	Ti	V	Zn
Halifax	18	9.8	17	30.1	19.4	32.7	10.6	23.2	33.5	33.1	17.1	9.1	8.7	12.3	22	55.9
Toronto	18	14.6	15.2	36.8	41.0	26.1	13.4	23.9	37.5	17.1	26.0	20.5	8.8	17.5	10.7	30.5
Beijing	14	16.5	24.1	24.9	15.7	19.3	16.9	28.9	14	21.1	28.9	13.9	21.5	20.7	31	18.2
SPARTAN	50	14.7	20.4	34.7	31.5	28.3	16.9	28.2	32.7	27.2	26.8	16.9	15.4	18.9	23.4	39

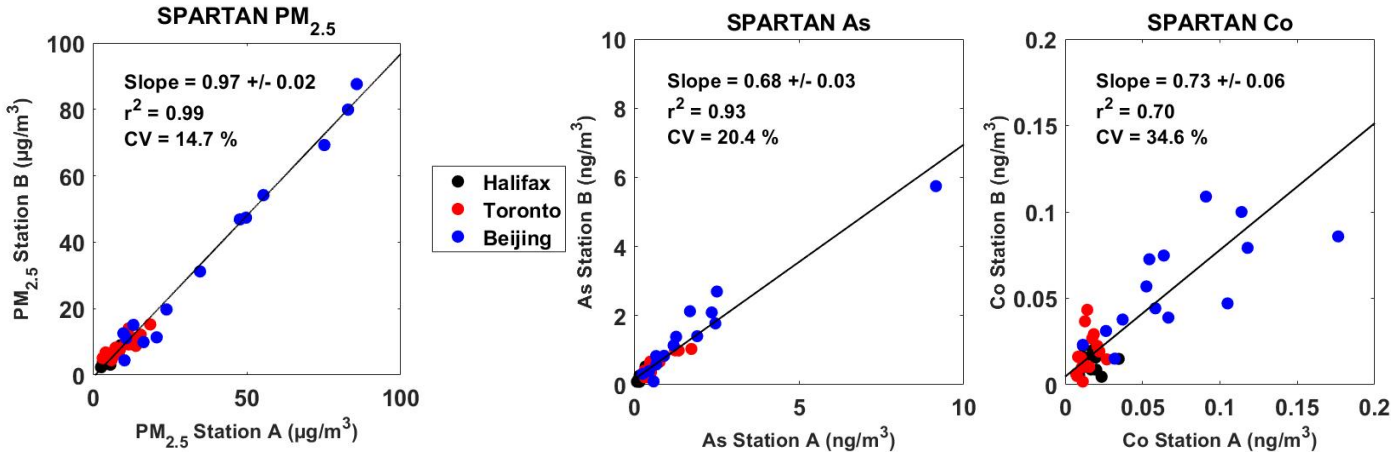

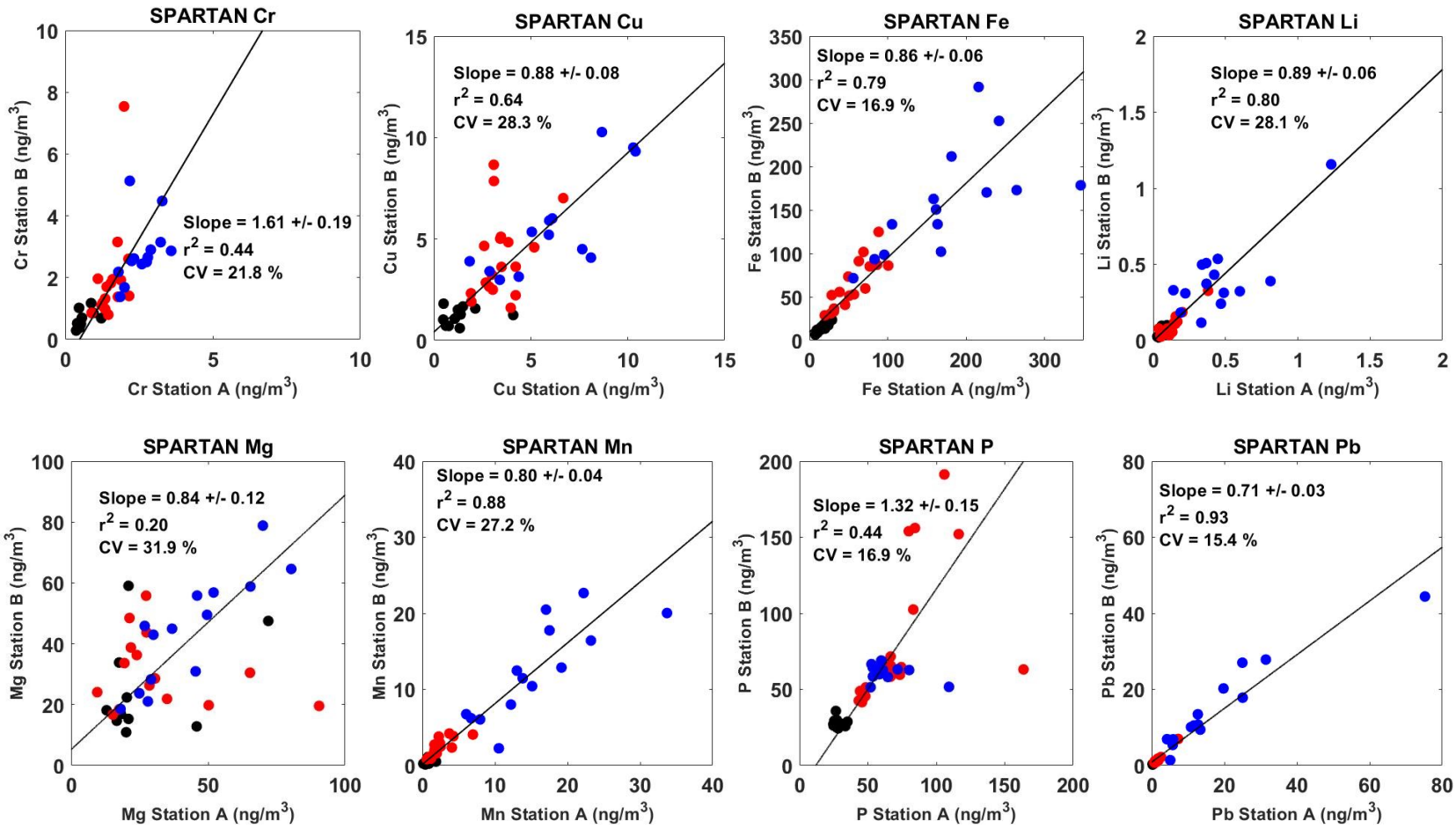
SPARTAN Cr
Slope = 1.61 +/- 0.19
r2 = 0.44
CV = 21.8 %
Cr Station B (ng/m3)
Cr Station A (ng/m3)
SPARTAN Cu
Slope = 0.88 +/- 0.08
r2 = 0.64
CV = 28.3 %
Cu Station B (ng/m3)
Cu Station A (ng/m3)
SPARTAN Fe
Slope = 0.86 +/- 0.06
r2 = 0.79
CV = 16.9 %
Fe Station B (ng/m3)
Fe Station A (ng/m3)
SPARTAN Li
Slope = 0.89 +/- 0.06
r2 = 0.80
CV = 28.1 %
Li Station B (ng/m3)
Li Station A (ng/m3)
SPARTAN Mg
Slope = 0.84 +/- 0.12
r2 = 0.20
CV = 31.9 %
Mg Station B (ng/m3)
Mg Station A (ng/m3)
SPARTAN Mn
Slope = 0.80 +/- 0.04
r2 = 0.88
CV = 27.2 %
Mn Station B (ng/m3)
Mn Station A (ng/m3)
SPARTAN P
Slope = 1.32 +/- 0.15
r2 = 0.44
CV = 16.9 %
P Station B (ng/m3)
P Station A (ng/m3)
SPARTAN Pb
Slope = 0.71 +/- 0.03
r2 = 0.93
CV = 15.4 %
Pb Station B (ng/m3)
Pb Station A (ng/m3)

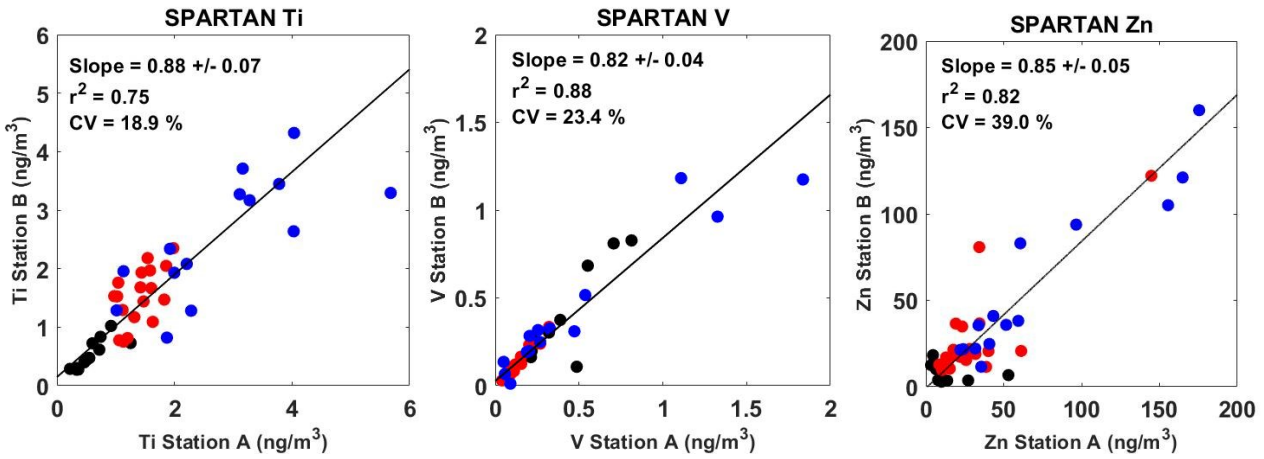

Figure 2.3: Individual plots of ICP-MS measured components at collocated sites in Halifax, Toronto, and Beijing used to estimate SPARTAN network uncertainties. CV shown in the plots represents the coefficient of variation upper bound calculated using Eq. 2.5.

**Note: some material for this Chapter has been adapted from "Large Global Variations in Measured Airborne Metal Concentrations Driven by Anthropogenic Sources" by Jacob McNeill et. al, published in* Scientific Reports *(December 2020)*

3 LARGE GLOBAL VARIATIONS IN MEASURED AIRBORNE METAL CONCENTRATIONS DRIVEN BY ANTHROPOGENIC SOURCES

The SPARTAN sampling network has collected and analyzed $PM_{2.5}$ data at ground sites since 2013, with 19 unique sites accounted for in the analysis detailed in this Chapter, and over 500 sampled $PM_{2.5}$ filters used. The dataset used in this investigation is exclusively samples that were analyzed for trace metal content by ICP-MS analysis, and sampling dates range from 2013-2019 depending on the site in question. The sampling breakdown for the sites used is shown in Table 3.1.

Table 3.1: Sampling breakdown for SPARTAN sites sampled and analyzed through ICP-MS. Sites are sorted by population density.

City	Population Density[a]	Mean PM2.5	PM2.5 Mass 1σ	Verified samples	First sample end date	Last sample end date	Sampled seasons[b]
Dhaka	80790	48.96	23.62	44	25-Oct-13	12-Oct-15	1,2,3,4
Bandung	22280	25.11	9.20	62	19-Jan-14	23-Dec-16	1,2,3,4
Hanoi	21430	47.13	17.81	7	09-Jun-15	09-Dec-17	1,3,4
Manila	20700	15.45	3.70	10	02-May-14	22-Oct-15	2,3,4
Beijing	18300	58.13	29.14	140	03-Sep-13	05-Oct-17	1,2,3,4
Pretoria	13400	18.31	6.86	4	27-Oct-15	29-May-16	2,4
Buenos Aires	9160	9.60	2.41	43	11-Oct-14	14-Oct-16	1,2,3,4
Singapore	5460	17.52	4.14	34	14-Apr-16	14-Dec-17	1,2,3,4
Halifax	5040	4.16	1.56	14	27-Aug-17	01-Apr-19	1,2,3,4
Toronto	3800	6.74	2.54	28	13-Jul-17	10-Mar-19	1,2,3,4
Kanpur	3250	102.83	90.77	11	23-Dec-13	26-Sep-14	1,2,3,4
Ilorin	1620	16.65	18.24	7	29-Jun-14	23-Apr-19	1,2,3,4
Rehovot	1440	14.22	7.50	35	22-Feb-15	03-Oct-18	1,2,3,4

City	Population Density[a]	Mean PM2.5	PM2.5 Mass 1σ	Verified samples	First sample end date	Last sample end date	Sampled seasons[b]
Sherbrooke	1190	5.65	2.23	11	06-Jul-17	20-Mar-19	1,2,3,4
Lethbridge	590	5.71	8.10	15	03-Sep-17	23-Jan-19	1,3,4
Atlanta	540	8.60	3.14	14	27-Jan-14	22-Apr-14	1,2
Kelowna	61	3.54	3.24	6	10-Nov-17	06-Mar-19	1,2,4
Mammoth Cave	13	14.20	7.71	21	09-Jun-14	12-Aug-14	3
Bondville	2	5.70	2.50	18	20-Aug-15	14-Apr-16	1,2,3,4

[a]Population density is for a 1 km radius based on NASA's Gridded Population of the World [29].

[b]For concision, seasons are labelled as such: 1 – Dec-Feb, 2 – Mar-May, 3 – Jun-Aug, 4 – Sept-Nov.

3.1 TRACE METAL CONTENT IN $PM_{2.5}$ AT SPARTAN SITES

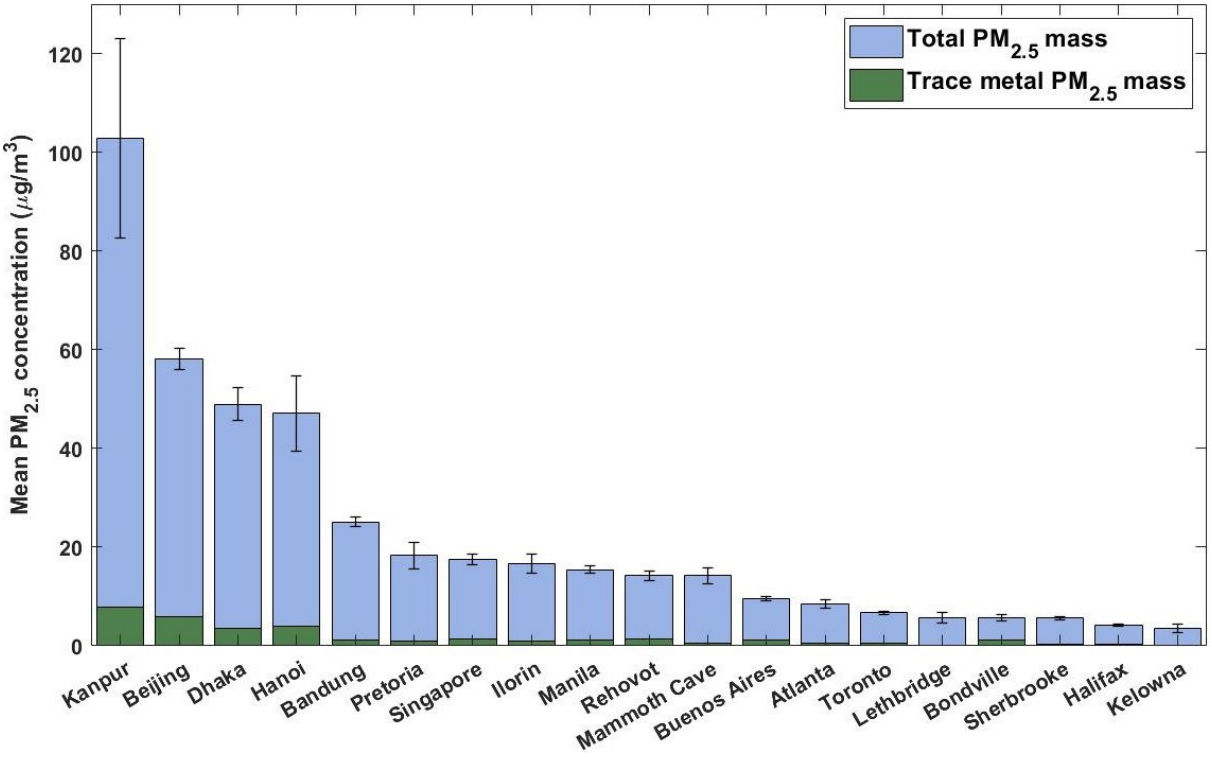

Figure 3.1: Mean $PM_{2.5}$ mass concentrations at SPARTAN sites with standard error bars shown. Overlaid green bars show total measured trace metal mean mass concentrations (from ICP-MS analysis) for each site.

The mean $PM_{2.5}$ mass concentrations at each SPARTAN site are shown in Figure 3.1, with standard error bars for each site mean. Of the 19 SPARTAN sites used in this investigation, Kanpur had the highest mean $PM_{2.5}$ levels at 102.8 ± 20.2 (SE) $\mu g/m^3$, followed by Beijing at 58.1 ± 2.2 $\mu g/m^3$, then Dhaka (49.0 ± 3.3 $\mu g/m^3$) and Hanoi (47.1 ± 7.6 $\mu g/m^3$). It should be noted that current SPARTAN sites located in Abu Dhabi and Seoul were not active during this period, and as such are not included in this analysis. Sites located in urban areas situated outside of North America generally had the highest levels of $PM_{2.5}$.

The one notable exception was the Mammoth Cave site, which had the 11th highest $PM_{2.5}$ levels. This can be explained through two aspects of the sampling; firstly, the site is located in a heavily wooded national park; sampling occurred in the summer when carbonaceous emissions are highest from biogenic sources, and secondary organic aerosol is prevalent.[81] Secondly, the site has the second-lowest percentage of its $PM_{2.5}$ mass present in the measured trace metal mass (4%), indicating other sources (i.e. biogenic) were dominant. Sites located in Canada generally had the lowest levels of $PM_{2.5}$, which is consistent with their intended categorization as low-PM environments.

Table 3.3 details the mean mass concentrations of 15 trace metals analyzed in $PM_{2.5}$ samples from SPARTAN sites. Elements above ICP-MS detection limits (detailed in Table 3.2) for >10% of samples were considered; Li, Co, Ag, and Ce did not satisfy this requirement, and as such are not discussed here. Whole-system uncertainties for the SPARTAN network were calculated in the same manner as previously discussed and shown in Table 2.2, with individual plots in Figure 2.3.

Table 3.2: SPARTAN network-wide statistics of fine fractions, element limits of detection, and samples above LOD for individual elements quantified by ICP-MS.

Element	Fine fraction[a]	LOD (ppb)[b]	Samples above LOD (%)
Mg	0.21	10	61
Al	0.23	4	78
Li	0.35	0.4	7
P	0.47	10	30
Ti	0.21	0.5	76
V	0.38	0.4	39
Cr	0.31	0.4	46
Mn	0.32	0.8	79
Fe	0.28	7	90
Co	0.18	0.4	2
Ni	0.48	0.4	50
Cu	0.37	0.7	75
Zn	0.48	0.6	79
As	0.56	0.4	47
Se	0.64	1	12
Ag	0.25	0.4	9
Cd	0.59	0.4	12
Ba	0.31	0.5	76
Ce	0.17	0.4	2
Pb	0.58	0.4	90

[a]Fine fraction for element x is reported as the geometric mean of the $\overline{x_{2.5}}/\overline{x_{10}}$ fractions for all SPARTAN sites.

[b]Limits of detection (LOD) are determined for the ICP-MS instrument for each individual element.

Table 3.3: Full elemental breakdown of mean mass concentrations of trace metals in $PM_{2.5}$ at SPARTAN sites. Mass concentrations of each trace metal are reported in ng/m^3. Total $PM_{2.5}$ mass concentrations are reported in µg/m^3.

	$PM_{2.5}$	K	Mg	P	Ti	V	Cr	Mn	Fe	Cu	Zn	As	Se	Cd	Ba	Pb
Mammoth Cave	14.2	74.8	28.0	55.7	1.01	0.78	1.20	1.84	83.2	3.68	8.5	0.26	0.28	0.05	3.12	0.90
Atlanta	8.6	27.8	11.5	105.3	1.24	0.18	4.20	0.71	51.5	3.67	9.3	0.56	0.54	0.02	5.41	1.08
Bandung	25.1	432.1	18.3	23.9	1.73	0.31	2.12	2.80	78.2	3.28	23.7	0.60	0.23	0.32	2.57	34.62
Beijing	58.1	962.6	177.3	151.1	11.18	2.30	4.39	23.84	394.7	26.73	101.5	7.12	67.40	3.29	21.81	41.30
Bondville	5.7	64.1	34.1	162.3	1.39	0.13	3.77	1.59	37.0	3.11	16.7	0.65	0.55	0.12	2.15	1.54
Buenos Aires	9.6	152.1	30.4	30.3	1.70	2.48	1.10	2.52	94.0	5.17	20.8	0.43	0.36	0.30	5.08	10.47
Dhaka	49.0	876.0	47.9	23.0	3.94	6.98	8.00	25.40	167.7	11.69	498.4	6.33	5.38	7.35	12.53	279.72
Halifax	4.2	40.0	17.8	1.1	0.25	0.23	0.39	0.36	10.8	0.76	3.7	0.14	0.07	0.00	0.75	0.49
Hanoi	47.1	1293.8	84.5	36.6	5.21	2.10	2.28	80.05	282.2	14.10	1178.8	8.11	3.00	4.25	7.13	141.04
Ilorin	16.6	355.6	15.5	5.1	0.88	0.61	47.96	4.51	182.4	0.94	12.9	0.22	0.14	0.06	0.90	4.27
Kanpur	102.8	3047.1	74.4	340.1	5.60	2.21	19.41	9.89	168.0	8.78	119.5	15.29	10.60	12.88	3.99	209.33
Kelowna	3.5	34.1	2.4	1.6	0.32	0.14	0.32	0.41	17.0	0.55	1.4	0.19	0.04	0.01	0.75	0.29
Lethbridge	6.2	56.3	6.4	1.5	0.30	0.03	0.25	0.68	18.5	0.76	1.9	0.17	0.14	0.03	0.85	0.38
Manila	15.4	253.3	20.3	34.4	1.30	2.32	2.97	3.17	111.2	2.93	29.4	0.33	0.96	0.25	2.31	5.89
Pretoria	18.3	220.0	14.8	37.5	1.66	0.44	0.80	5.78	105.2	2.28	27.5	1.00	0.54	0.10	2.54	4.88
Sherbrooke	5.7	48.3	5.0	4.3	0.45	0.03	0.20	0.92	16.7	0.73	4.2	0.26	0.10	0.02	0.58	1.08
Rehovot	15.4	135.2	79.9	11.4	2.18	2.95	1.56	2.82	123.5	3.22	12.8	0.26	0.34	0.09	3.69	4.64
Singapore	17.5	344.9	24.2	13.4	1.66	37.92	0.47	7.76	89.9	5.57	110.1	0.48	0.71	0.12	3.80	3.54
Toronto	6.7	71.0	12.0	9.7	0.83	0.09	0.72	1.59	46.5	2.71	10.7	0.31	0.29	0.04	3.82	1.38

3.2 CRUSTAL ENRICHMENT FACTORS

Of interest is the anthropogenic contribution to such trace metals in general. The relative enhancements of elements compared to natural crustal abundances was investigated through the application of enrichment factors, previously detailed in Section 2. Enrichment factors can be considered in three subsets: EF < 10, elements which we attribute to sources which are primarily crustal[82–84]; EF between 10 and 100, elements with mixed anthropogenic and natural sources; and EF > 100, elements with largely anthropogenic sources. Figure 3.2 displays the EF elemental breakdown for all SPARTAN sites as well as the site-specific PM_c-scaled EF results.

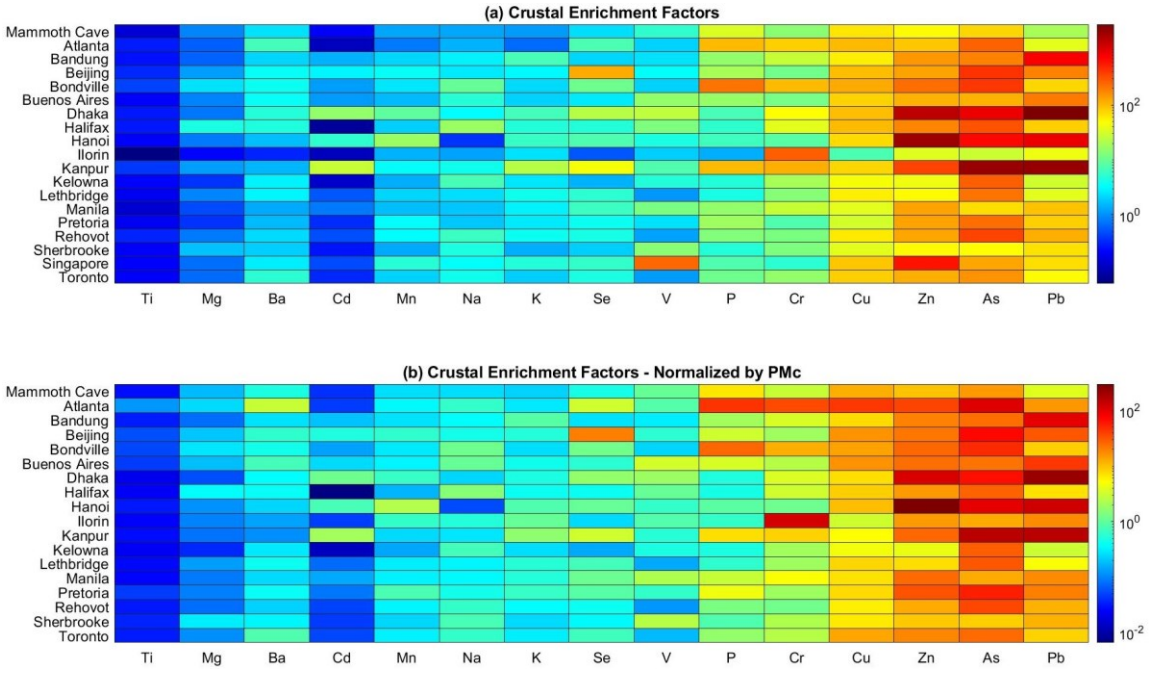

Figure 3.2: **(a) Crustal enrichment factors (EF) for $PM_{2.5}$ relative to crustal ratios of the given element and iron (Eq. 2.1), and (b) replacing measured iron with measured PM_c (Eq. 2.2). Elements are sorted by mean enrichment factor across all sites; sites are listed alphabetically. Singapore is not shown in the bottom plot due to unavailable PM_c data.**

Similar results when normalizing by either Fe or PM_c provides confidence in the analysis. Enrichment factors vary by orders of magnitude depending on element and location. The highest levels of enrichment are found in anthropogenically-dominant elements such as Pb, As, and Zn, and generally found at sites with the highest levels of $PM_{2.5}$. Of the four sites with the greatest $PM_{2.5}$ concentrations, elemental EF values >350 are found in Dhaka, Kanpur, and Hanoi for Pb, Zn, and As, and in Beijing for As. These enrichments highlight the effects of anthropogenic activities not only on total $PM_{2.5}$ but on trace metal $PM_{2.5}$ specifically, with potentially harmful levels of these heavy metals found in these high-PM cities.

Of the individual elements measured, two elements in particular demand further investigation: the carcinogenic metalloid As, and the toxic heavy metal Pb. These elements can originate from multiple industrial sources, including smelting, waste incineration, and coal burning.[12,14] Both elements have been shown to pose significant health risks, and as such regulatory bodies have created guidelines for their concentrations in air.

3.3 LEAD $PM_{2.5}$ CONCENTRATIONS AT SPARTAN SITES

The US National Ambient Air Quality (NAAQS) exposure limit for Pb is a 3-month mean concentration of 150 ng/m^3 [73], and multiple samples taken from the Kanpur and Dhaka sites exceeded these Pb concentrations – leading to mean concentrations over the US guideline. Figure 3.3 shows the lead concentrations measured in samples taken from the two sites, with the NAAQS guideline as a reference.

Comparing the two sites, Dhaka has both a higher mean (280 ng/m^3) than Kanpur (209 ng/m^3), and more samples measuring above the 150 ng/m^3 guideline (38% vs 30%). This contrasts with their respective levels of total $PM_{2.5}$, as mean $PM_{2.5}$ concentrations from Kanpur samples are roughly double those in Dhaka. The Dhaka site exhibits some seasonality, with peak Pb values occurring around January 2015 and generally high values in winter months, when mixed layer depths are shallow.

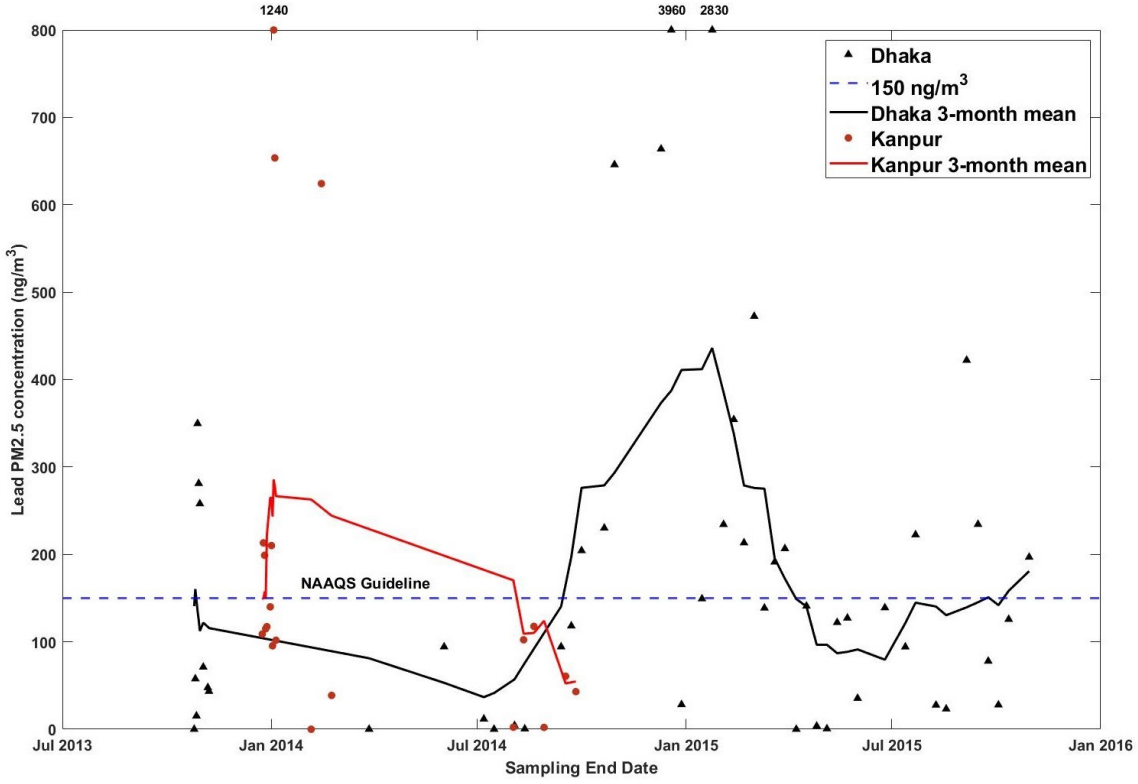

Figure 3.3: Concentrations of Pb in SPARTAN samples at Kanpur (red circles) and Dhaka (black triangles). Dotted blue line represents the NAAQS 3-month exposure guideline for lead concentrations (150 ng/m3). Samples are plotted by the final date of sampling, as sampling occurs over a time period of 9 days. Solid red (Kanpur) and black (Dhaka) lines represent 3-month rolling mean Pb concentrations.

3.4 ARSENIC $PM_{2.5}$ CONCENTRATIONS AT SPARTAN SITES

The second element of interest at SPARTAN sites is arsenic, as the World Health Organization recommends no safe level of arsenic exposure due to its carcinogenic risk. An estimated lifetime excess risk is 1:1,000,000 at 0.66 ng/m^3, or 1:100,000 at 6.6 ng/m^3 [85]. Arsenic is associated with industrial activities such as smelting, burning of coal, and waste incineration[38,86,87]. The majority of SPARTAN sites fall under the lower bound of that range, but multiple sites have substantial As concentrations. As shown in Figure 3.4, there are four sites with mean As concentrations near or above 6.6 ng/m^3 – Kanpur, Hanoi, Beijing, and Dhaka.

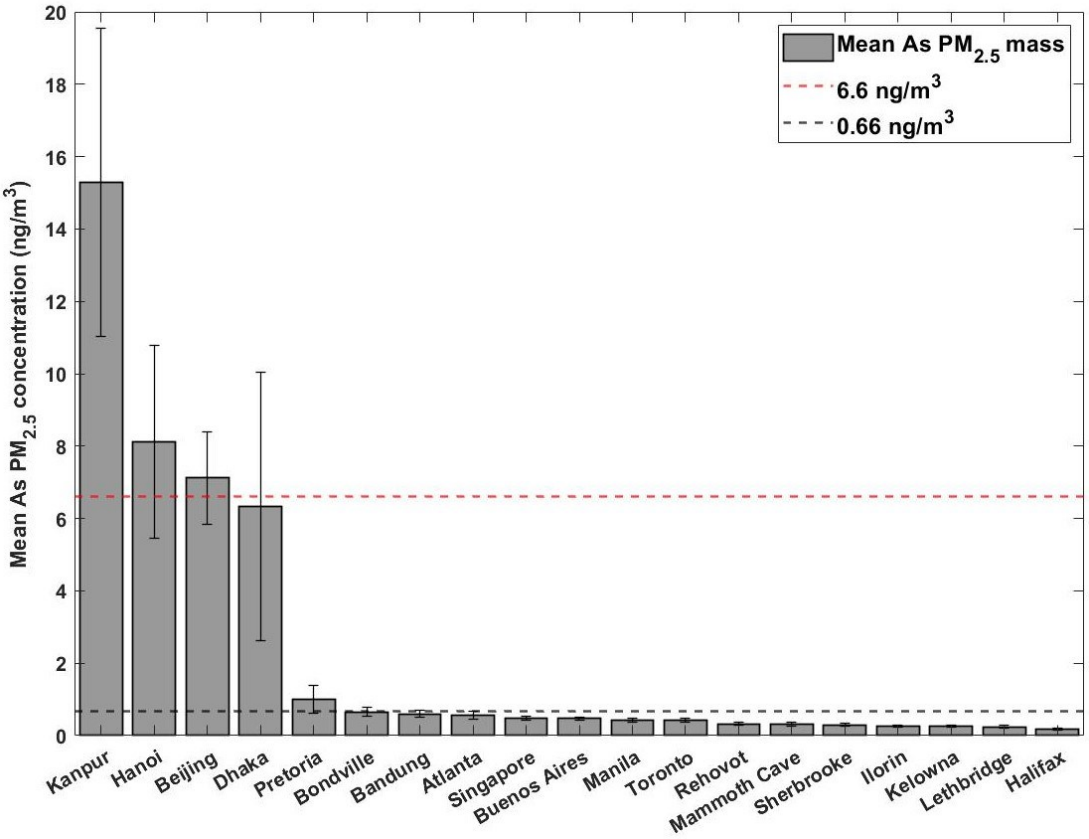

Figure 3.4: Concentrations of As in $PM_{2.5}$ samples taken from SPARTAN sites, with standard error bars shown. Dotted red line represents 1:100,000 excess lifetime risk of cancer due to As exposure (6.6 ng/m^3). Dotted black line represents 1:1,000,000 excess lifetime risk of cancer due to arsenic exposure (0.66 ng/m^3).

Kanpur has significantly higher As concentrations than any other SPARTAN site with 15.3 ng/m^3, which would translate to roughly 1:45,000 excess lifetime risk. The mean As mass concentrations for Hanoi, Beijing, and Dhaka were determined to be 8.1 ng/m^3, 7.1 ng/m^3, and 6.3 ng/m^3 respectively. These sites are also the four sites with the highest levels of $PM_{2.5}$, so it is not unexpected that they would have more significant amounts of trace metal $PM_{2.5}$ such as arsenic.

3.5 Relative Abundances vs. Mammoth Cave National Park

A complementary approach to understanding the levels of trace metals in fine PM at these sites is to compare them not only to the crustal abundance, but to another site with relatively low levels of these trace metals. Figure 3.5 shows the relative abundance (RA) of $PM_{2.5}$ trace metals at the eight SPARTAN sites with at least one elemental RA of 10 or greater, compared to a natural reference site, in this case the Mammoth Cave (M.C.) National Park site. The Mammoth Cave site has the second-lowest trace metal mass percentage of total $PM_{2.5}$ mass. Low trace metals and the natural environment of the site make it an insightful reference point against which to compare the various types of SPARTAN sites. Relative abundances for trace metal $PM_{2.5}$ are calculated using Eq. 3.1 and are unitless.

$$RA_X = [X]_{\text{Site}} / [X]_{\text{M.C.}} \qquad \text{Eq. 3.1}$$

Sites with an elemental RA of 10 or greater are shown in the figure below to highlight particular areas and species of note. The full set of relative abundances is shown in Table

3.4. A similar calculation using the $PM_{2.5}$-relative elemental concentrations instead of the absolute concentrations was performed using Eq. 3.2, shown in

$$RA_{Xrel} = ([X]_{\text{Site}}/PM_{2.5_{site}})/([X]_{\text{M.C.}}/PM_{2.5_{M.C.}}) \qquad \text{Eq. 3.2}$$

Generally, combustion-related elemental concentrations increase together, as do crustal components. Particularly high RA values (12-311) of anthropogenic elements Zn, As, Pb, and Cd are found for Kanpur, Beijing, Dhaka, and Hanoi; these abundances are in alignment with the crustal enrichments seen for these heavy metals at these sites, and with the higher $PM_{2.5}$ levels at these sites.

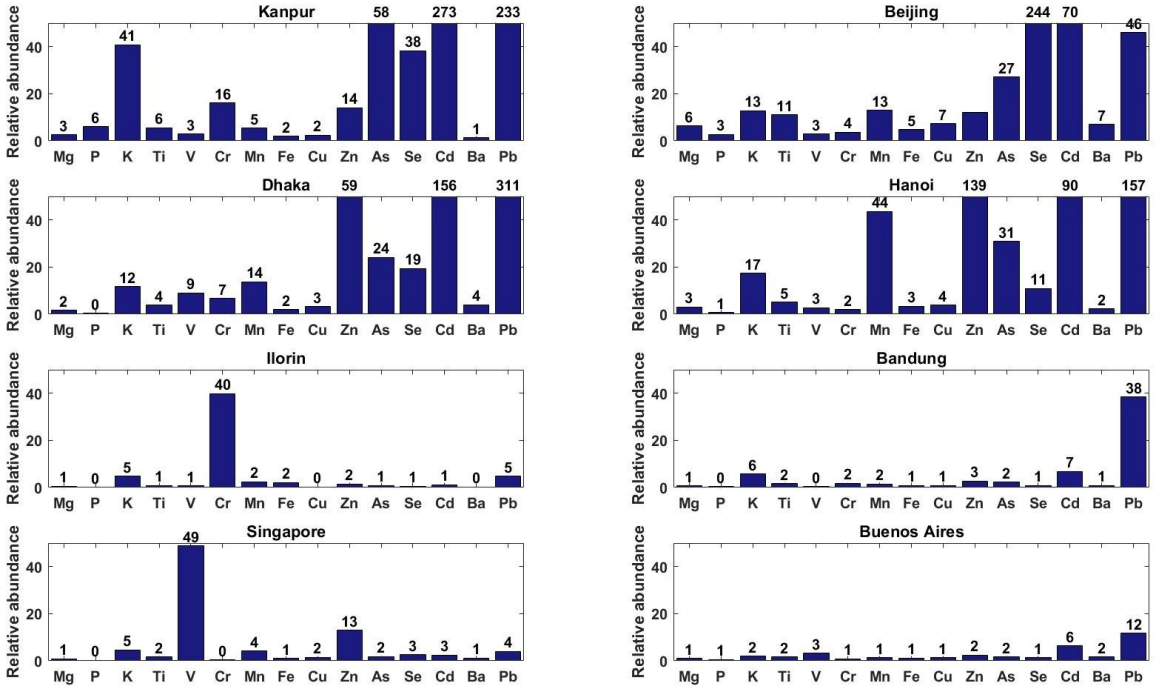

Figure 3.5: Relative abundances (unitless) of trace metals in $PM_{2.5}$ of the SPARTAN sites with at least one element with RA of 10 or greater. Abundances are relative to the natural, low-trace metal $PM_{2.5}$ Mammoth Cave site. Sites are sorted by total $PM_{2.5}$ mass concentrations L-R, then top to bottom.

Table 3.4: Relative abundances of trace metals at SPARTAN sites as compared to the low-trace metal reference site of Mammoth Cave. Values shown are unitless.

	K	Mg	P	Ti	V	Cr	Mn	Fe	Cu	Zn	As	Se	Cd	Ba	Pb
Atlanta	0.4	0.4	1.9	1.2	0.2	3.5	0.4	0.6	1.0	1.1	2.1	2.0	0.3	1.7	1.2
Bandung	5.8	0.7	0.4	1.7	0.4	1.8	1.5	0.9	0.9	2.8	2.3	0.8	6.8	0.8	38.5
Beijing	12.9	6.3	2.7	11.1	3.0	3.7	13.0	4.7	7.3	12.0	27.1	243.8	69.7	7.0	45.9
Bondville	0.9	1.2	2.9	1.4	0.2	3.1	0.9	0.4	0.8	2.0	2.5	2.0	2.5	0.7	1.7
Buenos Aires	2.0	1.1	0.5	1.7	3.2	0.9	1.4	1.1	1.4	2.5	1.6	1.3	6.4	1.6	11.6
Dhaka	11.7	1.7	0.4	3.9	9.0	6.7	13.8	2.0	3.2	58.8	24.1	19.5	155.7	4.0	311.0
Halifax	0.5	0.6	0.0	0.2	0.3	0.3	0.2	0.1	0.2	0.4	0.5	0.3	0.0	0.2	0.5
Hanoi	17.3	3.0	0.7	5.2	2.7	1.9	43.6	3.4	3.8	139.1	30.9	10.9	90.1	2.3	156.8
Ilorin	4.8	0.6	0.1	0.9	0.8	39.9	2.5	2.2	0.3	1.5	0.8	0.5	1.2	0.3	4.7
Kanpur	40.8	2.7	6.1	5.5	2.8	16.2	5.4	2.0	2.4	14.1	58.2	38.3	273.0	1.3	232.7
Kelowna	0.5	0.1	0.0	0.3	0.2	0.3	0.2	0.2	0.2	0.2	0.7	0.1	0.1	0.2	0.3
Lethbridge	0.8	0.2	0.0	0.3	0.0	0.2	0.4	0.2	0.2	0.2	0.7	0.5	0.6	0.3	0.4
Manila	3.4	0.7	0.6	1.3	3.0	2.5	1.7	1.3	0.8	3.5	1.2	3.5	5.3	0.7	6.6
Pretoria	2.9	0.5	0.7	1.6	0.6	0.7	3.1	1.3	0.6	3.2	3.8	2.0	2.1	0.8	5.4
Rehovot	0.6	0.2	0.1	0.4	0.0	0.2	0.5	0.2	0.2	0.5	1.0	0.4	0.5	0.2	1.2
Sherbrooke	1.8	2.9	0.2	2.2	3.8	1.3	1.5	1.5	0.9	1.5	1.0	1.2	1.9	1.2	5.2
Singapore	4.6	0.9	0.2	1.6	48.7	0.4	4.2	1.1	1.5	13.0	1.8	2.6	2.5	1.2	3.9
Toronto	1.0	0.4	0.2	0.8	0.1	0.6	0.9	0.6	0.7	1.3	1.2	1.0	0.9	1.2	1.5

Table 3.5: $PM_{2.5}$-relative elemental concentrations at SPARTAN sites compared to relative elemental concentrations at the low-trace metal reference site of Mammoth Cave. Values shown are unitless.

	K	Mg	P	Ti	V	Cr	Mn	Fe	Cu	Zn	As	Se	Cd	Ba	Pb
Atlanta	0.6	0.7	3.1	2.0	0.4	5.8	0.6	1.0	1.6	1.8	3.6	3.2	0.7	2.9	2.0
Bandung	3.3	0.4	0.2	1.0	0.2	1.0	0.9	0.5	0.5	1.6	1.3	0.5	3.6	0.5	21.8
Beijing	3.1	1.5	0.7	2.7	0.7	0.9	3.2	1.2	1.8	2.9	6.7	58.8	16.1	1.7	11.2
Bondville	2.1	3.0	7.3	3.4	0.4	7.8	2.2	1.1	2.1	4.9	6.2	4.9	6.0	1.7	4.3
Buenos Aires	3.0	1.6	0.8	2.5	4.7	1.4	2.0	1.7	2.1	3.6	2.4	1.9	8.9	2.4	17.2
Dhaka	3.4	0.5	0.1	1.1	2.6	1.9	4.0	0.6	0.9	17.0	7.1	5.6	42.6	1.2	90.1
Halifax	1.8	2.1	0.1	0.8	1.0	1.1	0.7	0.4	0.7	1.5	1.8	0.8	0.0	0.8	1.8
Hanoi	5.2	0.9	0.2	1.6	0.8	0.6	13.1	1.0	1.2	41.8	9.4	3.2	25.6	0.7	47.2
Ilorin	4.1	0.5	0.1	0.7	0.7	34.2	2.1	1.9	0.2	1.3	0.7	0.4	1.0	0.2	4.1
Kanpur	5.6	0.4	0.8	0.8	0.4	2.2	0.7	0.3	0.3	1.9	8.1	5.2	35.6	0.2	32.1
Kelowna	1.8	0.3	0.1	1.3	0.7	1.1	0.9	0.8	0.6	0.7	3.0	0.6	0.8	1.0	1.3
Lethbridge	1.7	0.5	0.1	0.7	0.1	0.5	0.8	0.5	0.5	0.5	1.5	1.1	1.4	0.6	1.0
Manila	3.1	0.7	0.6	1.2	2.7	2.3	1.6	1.2	0.7	3.2	1.2	3.2	4.6	0.7	6.0
Pretoria	2.3	0.4	0.5	1.3	0.4	0.5	2.4	1.0	0.5	2.5	3.0	1.5	1.6	0.6	4.2
Rehovot	1.6	0.4	0.2	1.1	0.1	0.4	1.2	0.5	0.5	1.2	2.5	0.9	1.0	0.5	3.0
Sherbrooke	1.7	2.6	0.2	2.0	3.5	1.2	1.4	1.4	0.8	1.4	0.9	1.1	1.7	1.1	4.8
Singapore	3.7	0.7	0.2	1.3	39.4	0.3	3.4	0.9	1.2	10.5	1.5	2.1	1.9	1.0	3.2
Toronto	2.0	0.9	0.4	0.0	0.0	1.3	1.8	1.2	1.6	2.7	2.5	2.2	1.7	2.6	3.2

Examining the relative abundances on a site-specific basis reveals more local information – one notable instance being the Beijing site, which shows markedly elevated levels of selenium compared to any other site. Chinese coal has been found to be particularly rich in selenium[88], which in concert with the large quantity of coal burned in China implies coal-burning as a major anthropogenic source of selenium $PM_{2.5}$. Coal emissions in China have also been shown to contain high levels of As, Cd, and Pb[89], all of which are significantly elevated by RA in the $PM_{2.5}$ samples from Beijing.

There are a few isolated, notable RA values at the Bandung and Ilorin sites that can be linked to specific regional industries. Bandung has highly elevated Pb (RA of 38, EF > 700), even after the phasing out of leaded gasoline in 2006.[90] One likely contributor to the extremely high Pb levels is lead smelting, as Indonesia is one of the largest lead acid battery recyclers in Asia.[91] Rapidly growing numbers of lead smelters produce large amounts of Pb-enhanced emissions, the transport of which could explain the elevated lead levels seen at the Bandung site. The Ilorin site shows abundant levels of Cr (RA of 40, EF > 260); this may be associated with the prevalent tanning industry in the region, in which chromium compounds are used prominently. Analysis of effluents from Nigerian tanneries found high levels of Cr present[92], and high levels of the metal in $PM_{2.5}$ imply that some of this Cr is being converted to or released in particulate form.

Singapore has significant enrichment of V (49), which likely stems from the nearby burning of shipping fuel, with the Port of Singapore being one of the busiest ports in the world. Proximity to petroleum refineries is another likely contributor to these elevated V levels[93], as the Singapore site is located approximately 10 km east-northeast of Jurong Island, an

industrialized artificial island home to several refineries.[94] Significantly enhanced levels of V in Singapore can also be seen in the crustal EFs (EF > 240, the highest for V of any SPARTAN site), which further validates the key impact of nearby anthropogenic emissions. The influence of these and other nearby anthropogenic activities (e.g. vehicular traffic and metal production facilities) is also seen in enhanced levels of Zn, with an RA value of 13 and EF > 600. Unlike some of the other regions with high $PM_{2.5}$ and significant anthropogenic activity, Singapore does not exhibit large relative abundances for other anthropogenically dominant elements such as Pb, As, and Cr. This is likely due to the near-total absence of coal-burning in the region, as Singapore relies heavily on natural gas for energy purposes.[94]

Two non-North American sites did not exhibit any RA values of 10 or higher: Manila and Rehovot. This merits attention as Manila in particular is a densely populated city yet shows no significantly higher levels of trace metals than our natural site in Mammoth Cave. One partial explanation is that Manila has relatively low $PM_{2.5}$ mass concentrations among the non-North American sites (8^{th} out of 11 sites). For Rehovot, the sampling site is the least densely populated non-North American site, which would align with the generally low amounts of trace metals observed at that location. Of the North American sites, Toronto, Bondville, Sherbrooke, Atlanta, Halifax, Kelowna, and Lethbridge all had RA values below 5 for all elements measured. This aligns well with expectations that these sites should generally have less PM pollution, especially for the Canadian MAPLE sites designated as low-PM environments.

Although SPARTAN does not yet have sites in Europe, we surveyed prior measurements from the region to place our findings elsewhere in context. We find that at European background reference sites, heavy metal concentrations tended to be lower than at SPARTAN sites in densely populated regions.[95,96] These findings reinforce our conclusions about the enrichment of heavy metals compared with background reference sites.

**Note: this Chapter has been adapted from "Large Global Variations in Measured Airborne Metal Concentrations Driven by Anthropogenic Sources" by Jacob McNeill et. al, published in* Scientific Reports *(December 2020)*

4 XRF ANALYSIS OF SPARTAN SAMPLES

4.1 DEVELOPMENT OF XRF ANALYSIS PROCEDURE

Beginning in 2019, XRF analysis was introduced into the workflow of the SPARTAN network in order to quantify trace metal concentrations in ambient particulate matter, replacing the previously used and discussed ICP-MS analysis. The rationale for the switch is discussed earlier in this work (see section 1.5) but was primarily motivated by the tendency of ICP-MS digestion (specifically with methods available to the network at the time) to underreport certain crustal elements, such as aluminum. In addition, there are other incentives to use XRF analysis for SPARTAN trace metal concentrations: the non-destructive nature of the technique allows for both repeat measurements and for samples to be easily used in other analysis down the line, and the ease of sample preparation and analysis allows for more efficient throughput of measurements.

4.1.1 XRF Instrument Setup

XRF analysis took place in the SPARTAN laboratory using the Epsilon 4 benchtop energy dispersive X-ray fluorescence (EDXRF) analyzer from Malvern Panalytical, which operates using a silver anode X-ray tube and a high-resolution silicon drift detector. The experimental setup for XRF analysis in the SPARTAN lab is shown in Figure 4.1. The instrument holds a 10-slot sample changer and uses a spinner arm (shown below in Figure 4.1e) to rotate the sample currently under analysis. SPARTAN filters were placed loaded

side-down on a custom polylactic acid 3-D printed filter holder, and then placed in a stainless-steel sample holder inside the Epsilon 4 sample changer.

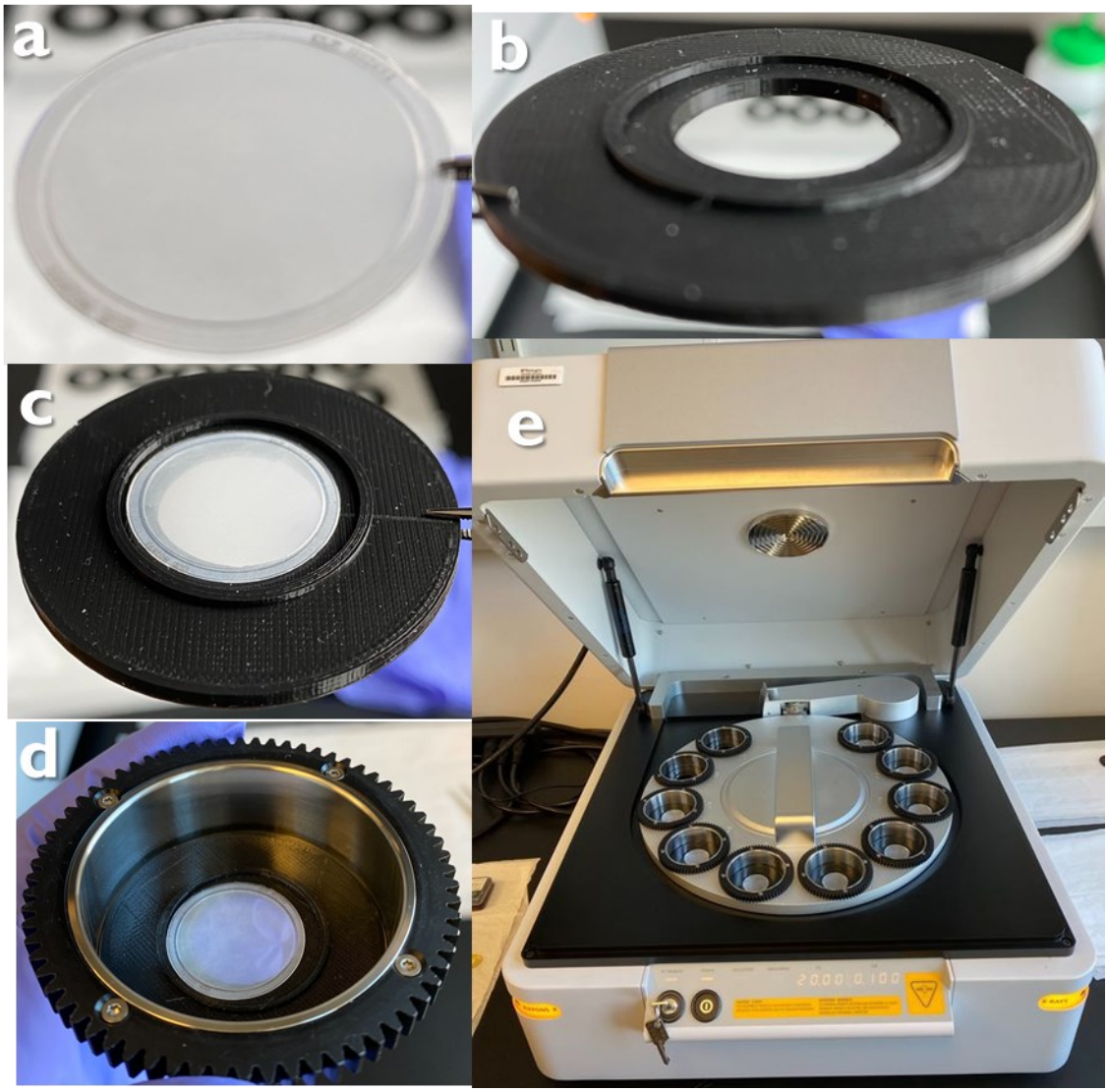

Figure 4.1: Experimental setup of XRF analysis in the SPARTAN laboratory. (a) Teflon PM filter, to be placed deposit side down into (b) custom 3-D printed polylactic acid (PLA) filter holder. (c) Assembled filter and holder, to be placed into stainless steel filter holder. (d) Full assembly to be loaded into (e) 10-slot sample changer, shown here inside the open Epsilon 4 instrument.

The 3-D printed filter holders were created using the Jubel Hall Makerspace facilities at Washington University in St. Louis, and were designed to ensure that the smaller Teflon filters used by SPARTAN (25mm outer diameter) could be used in the stainless-steel

sample holders from Malvern Panalytical intended for larger air filters (47mm). In order to ensure that all sizes of filters were held in the sample changers at the same vertical distance from the X-ray beam, equivalent 3-D printed filter holders were created for 47mm and 36mm standards used in the calibration of the instrument.

Calibration of the Epsilon 4 was performed using over 60 single-element and multi-element standards for 25 unique elements of interest, which included quantitatively loaded 47mm filters obtained from the University of California, Davis' Air Quality Research Center, 36mm thin-film standards from Micromatter Technologies, and the National Institute of Standards and Technology's Standard Reference Material 2783.

The breakdown of the standards used is shown in Table 4.1. Four unique multi-element standards (loaded with 20 or more elements of interest) were used in calibration to replicate the diverse elemental loadings seen on sampled SPARTAN filters.

Table 4.1: Breakdown of standards used in the calibration of the Epsilon 4 XRF analyzer.

Element	Standard Source[a]			Total Standards	Calibration Range (µg/cm2)	
	UCD	MM	NIST			
Al	6	2	1	9	0.356	5.52
As	3	0	1	4	0.0012	0.522
Ca	6	0	1	7	0.356	5.79
Cd	3	0	0	3	0.024	0.104
Ce	6	0	0	6	1.1	28.69
Cl	9	2	0	11	0.012	13.04
Co	3	2	1	6	0.0008	5.4
Cr	3	2	1	6	0.0136	5.3
Cu	3	2	1	6	0.035	6.7
Fe	6	0	1	7	0.356	4.26
K	6	2	1	9	0.3	6.21
Mg	3	2	1	6	0.119	2.7
Mn	3	2	1	6	0.032	7.5
Ni	3	2	1	6	0.0024	6.4

Element	Standard Source[a]			Total Standards	Calibration Range (µg/cm2)	
	UCD	MM	NIST			
Pb	6	0	1	7	0.0318	2.63
Rb	3	0	1	4	0.0024	0.104
S	12	0	1	13	0.105	10.55
Sb	0	2	1	3	0.0072	6.8
Se	3	2	1	6	0.059	5.3
Si	6	2	1	9	0.65	5.96
Sn	0	2	0	2	1.4	7.1
Sr	3	0	0	3	0.024	0.104
Ti	6	0	1	7	0.024	8.54
V	6	0	1	7	0.0049	2.86
Zn	6	0	1	7	0.031	3.6

[a]Standards were sourced from University of California, Davis' Air Quality Research Center (UCD), Micromatter Technologies (MM) and the National Institute of Standards and Technology (NIST).

Samples were measured directly using the Epsilon 4 software using X-ray condition sets adapted from Malvern Panalytical for air filter analysis: these conditions are listed in Table 4.2. To briefly summarize the aspects of the conditions, the voltage (kV) of the X-ray cathode tube controls the energy of X-rays created, the current (µA) of the cathode tube affects the quantity of X-rays produced, the filter is used to selectively filter out X-rays outside of the desired energy range, and the medium used affects background noise.

Table 4.2: Condition sets used in E4 software for XRF analysis of SPARTAN filters.

Condition name	kV	µA	Filter name	Medium	Detector mode	Analysis time (s)	Elements analyzed
<Fe-Pb>	50	300	Ag	Air	Normal	540	Fe, Co, Ni, Cu, Zn, As, Se, Rb, Sr, Pb
<K-La>	12	1250	Al-50	Air	Normal	540	K, Ca, Ti
<Mg-Cl>	9	1666	Ti	Helium	Normal	720	Mg, Al, Si, S, Cl
<Pd-Sb>	50	300	Cu-500	Air	Normal	540	Pd, Cd, Sn, Sb
<V-Mn,Ce>	20	750	Al-200	Air	Normal	540	V, Cr, Mn, Ce

These conditions are designed in order to maximize detection of the characteristic fluorescence of the elements in the condition set – heavier elements will typically be subjected to higher energy X-rays (i.e. high kV values) that are necessary to induce their transitions, while lighter elements require lower energy X-rays (low kV values) for their specific transitions. This relationship is essentially inverted in terms of the quantity of X-rays used, as lighter elements generally have lower fluorescence yield, and require more X-rays (i.e. high μA values) in order to obtain enough characteristic fluorescence to be quantified, while heavy elements with high fluorescence yield require fewer X-rays (low μA values) to obtain sufficient fluorescence without overloading the instrument detector.

In condition set <Mg-Cl>, ultra-pure helium (UHP6.0, 99.999% He, Airgas) is used to reduce background noise, as light elements (low atomic weight) produce less X-ray fluorescence than heavier elements. The signal-to-noise enhancement observed from use of helium in this condition set is significant enough to merit the relatively costly use of helium – for heavier elements, the signal-to-noise enhancement is not significant and therefore use of helium is conserved to only the <Mg-Cl> condition set. This set also has increased measurement time for improved signal resolution.

4.1.2 Limit of Detection (LOD) Determination

After the programming setup and calibration of the Epsilon 4 instrument was completed, the elemental detection limits of the method were determined. The quantification of 25 unique elements leads to 25 unique detection limits, detailed below in Table 4.3. Two metrics are used and reported here – the first is the limit of detection (LOD), defined in Eq.

4.1, where s is the standard deviation of the measured concentrations from a set of nine lab blanks for the element of interest:

$$LOD = 3 * s \quad \text{Eq. 4.1}$$

The second reported metric is acceptance limit, which is defined in Eq. 4.2, where $\bar{x}$ is the mean concentration of the set of nine lab blanks for the element of interest:

$$Acceptance\ limit = LOD + \bar{x}, \text{if } \bar{x} > 0 \quad \text{Eq. 4.2}$$

In practical terms, the LOD is used to account for instrument noise using the 3σ rule, wherein ~99% of normally distributed values are found within three standard deviations of the mean value, and has been shown to correspond to a confidence level of ~90%.[97]

Table 4.3: Limits of detection and acceptance limits for 25 unique elements analyzed through XRF, as well as percentage of recorded SPARTAN XRF samples above acceptance limits. Values reported are in µg/cm2 (mass deposited per unit area).

Element	LOD	Acceptance Limit	Samples over AL (%)	Element	LOD	Acceptance Limit	Samples over AL (%)
Al	0.0072	0.0078	100	**As**	0.0021	0.0021	78
Si	0.0213	0.0257	100	**Co**	0.0012	0.0013	32
S	0.0018	0.0029	100	**Cr**	0.0018	0.0018	65
Cl	0.0486	0.0486	38	**Cu**	0.0042	0.0074	57
K	0.0642	0.1009	96	**Mg**	0.0765	0.0765	83
Ca	0.0345	0.041	94	**Mn**	0.0015	0.0015	97
Ti	0.0031	0.031	40	**Ni**	0.0012	0.0017	57
V	0.0009	0.0012	66	**Sb**	0.0513	0.0579	3
Fe	0.0078	0.0078	100	**Rb**	0.0048	0.0056	22
Zn	0.0015	0.0027	98	**Sr**	0.0072	0.0077	20
Ce	0.003	0.003	45	**Cd**	0.0147	0.0147	7
Pb	0.0054	0.006	62	**Se**	0.0006	0.0006	71
Sn	0.0549	0.0818	3				

The acceptance limit is used to ensure that any potential loadings of elements on the lab blanks are accounted for before reporting loadings on sampled filters – an example being potassium, where the difference between the LOD and acceptance limit is roughly 30%. These values are used to filter SPARTAN sample data, with only elemental concentrations above the relevant acceptance limit carried through for further data analysis. Elements above XRF acceptance limits for >10% of samples were considered; Sb, Cd, and Sn did not satisfy this requirement, and as such are not further discussed here.

4.2 Overview of XRF Results for SPARTAN Sites

Due to the relatively recent introduction of XRF analysis into SPARTAN protocols, there are fewer samples collected and characterized than the previous ICP-MS analysis, but by no means is it an insignificant set – there are over 220 $PM_{2.5}$ filters that have been used in this analysis. The breakdown for the sampling at the sites used can be found in Table 4.4. It should be noted that the Seoul and Abu Dhabi sites were not included in ICP-MS analysis, while the Atlanta, Bondville, Buenos Aires, Kanpur, Kelowna, Mammoth Cave, Manila, and Pretoria sites were not analyzed through XRF due to either site retirement or insufficient sampling.

The mean $PM_{2.5}$ mass concentrations measured from samples during the analysis period explored here are plotted in Figure 4.2, with standard error bars shown, and the total mass of the trace components analyzed through XRF overlaid in green.

Table 4.4: Sampling breakdown for SPARTAN sites sampled and analyzed through XRF. Sites are sorted by population density.

City	Population Density[a]	Mean PM2.5	PM2.5 Mass 1σ	Verified samples	First sample end date	Last sample end date	Sampled seasons[b]
Dhaka	80790	123.19	22.6	6	13-Nov-19	19-Dec-19	1,4
Bandung	22280	36.66	11.0	22	12-Jul-19	17-Jul-20	1,3,4
Hanoi	21430	28.19	8.5	13	05-Dec-18	12-Aug-19	1,2,3
Seoul	18362	21.18	7.6	6	10-May-19	24-Jun-19	2,3
Beijing	18300	24.03	8.3	29	16-May-19	24-Jul-20	1,2,3,4
Singapore	5460	23.93	10.9	13	15-Jul-19	17-Dec-19	1,3,4
Halifax	5040	3.06	1.0	24	24-Aug-19	03-May-20	1,2,3,4
Toronto	3800	6.45	1.5	12	30-Mar-19	12-Aug-19	2,3
Ilorin	1620	39.76	66.3	18	22-May-19	19-Jan-20	2,3,4
Rehovot	1440	13.01	3.9	20	22-Feb-19	27-Mar-20	1,2,3
Sherbrooke	1190	4.86	1.9	25	11-Apr-19	22-May-20	1,2,3,4
Lethbridge	590	5.04	1.9	13	17-Mar-19	31-Aug-19	2,3
Abu Dhabi	31	38.61	10.7	34	05-May-19	18-Sep-20	1,2,3,4

[a]Population density is for a 1 km radius based on NASA's Gridded Population of the World [29].

[b]For concision, seasons are labelled as such: 1 – Dec-Feb, 2 – Mar-May, 3 – Jun-Aug, 4 – Sept-Nov.

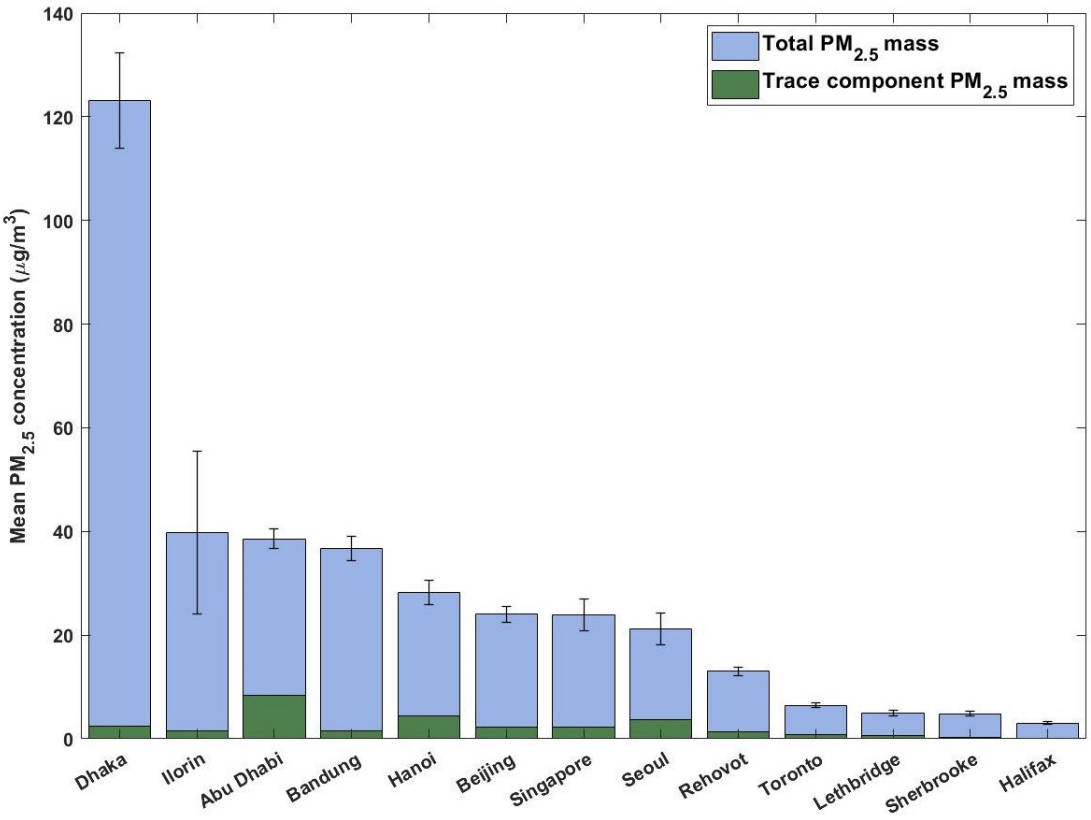

Figure 4.2: Mean $PM_{2.5}$ mass concentrations at SPARTAN sites with standard error bars shown. Overlaid green bars show total measured trace metal mean mass concentrations (from XRF analysis) for each site.

As can be seen, the site with the highest levels of ambient $PM_{2.5}$ from this analysis is Dhaka by more than a factor of threefold compared to the next highest site (123 $\mu g/m^3$ vs 40 $\mu g/m^3$ in Ilorin). This is likely due to the period of sampling for the Dhaka site, which sampled only in the winter months (November-December) in this analysis. Seasonality of $PM_{2.5}$ in Dhaka has been discussed in section 3.3, wherein the Pb $PM_{2.5}$ levels rose starkly in those winter months due to shallow mixed layer depths and increased combustion activities. Total $PM_{2.5}$ concentrations during these months have been shown[98] to rise well over 100 $\mu g/m^3$ in Dhaka, so this level of ambient $PM_{2.5}$ is well within the range expected to be observed. The disparity between the $PM_{2.5}$ mean mass concentrations at the site through the XRF analysis time period and the ICP-MS analysis time period (123 $\mu g/m^3$ vs 49 $\mu g/m^3$) also highlights this seasonality, as the previous analysis included samples ranging across all seasons.

Temporal factors also impact the site with the second-highest mean $PM_{2.5}$ concentrations, as the Ilorin site demonstrated mean $PM_{2.5}$ levels of 40 $\mu g/m^3$, but also exhibited the largest $PM_{2.5}$ mass standard deviation of all sites. This can be traced to the time period of sampling, as samples taken from the Nigerian site during the Harmattan dust season in West Africa (roughly Dec-Mar) are significantly higher than those taken during the remaining months of the year, leading to the large standard deviation. The mean $PM_{2.5}$ concentration for the site during the Dec-Jan-Feb season was nearly tenfold higher than the mean concentration for samples taken from May-Nov (97 $\mu g/m^3$ vs 11 $\mu g/m^3$). These seasonal influences on $PM_{2.5}$ mass concentration provide important context to the values shown in Figure 4.2.

As might be expected, Canadian sites demonstrated the lowest mass concentrations of $PM_{2.5}$, which is consistent with the characterization of these sites as low-PM environments. It can also be seen that the $PM_{2.5}$ mass at SPARTAN sites correlates very well to the population density of the site (Table 4.4), with the exceptions of Ilorin which has been discussed, and Abu Dhabi, another site in an arid region with significant potential dust impact. The remainder of the international SPARTAN sites exhibit ambient $PM_{2.5}$ mass concentrations ranging from ~15-40 $\mu g/m^3$, all of which are greater than the WHO air quality guideline of 10 $\mu g/m^3$ annual mean $PM_{2.5}$ concentration. This indicates that air quality remains a health concern in many of the locations of SPARTAN sampling sites, and validates the continuing assessment of $PM_{2.5}$ in these regions.

One promising development from continued assessment of $PM_{2.5}$ mass concentrations at SPARTAN sites is at the Beijing site specifically, which showed a nearly 60% reduction in mean $PM_{2.5}$ concentration compared to the previous ICP-MS analysis (58.1 $\mu g/m^3$ to 24.0 $\mu g/m^3$). While the time period of sampling may play a role in this change, both analyses included samples from all four seasons giving credence to this decrease. Notably, the mean $PM_{2.5}$ masses from the XRF analysis are nearly identical before and after COVID-19 lockdowns (25.3 $\mu g/m^3$ vs 23.0 $\mu g/m^3$), indicating that shutdowns were not a driving factor in this change.

The detailed elemental breakdown of the sampled $PM_{2.5}$ at each of the SPARTAN locations is shown in Table 4.5, along with the site mean $PM_{2.5}$ mass concentrations measured over the period of analysis for XRF. 22 unique elemental concentrations are reported for each of the 13 sites with XRF analysis.

Table 4.5: Full elemental breakdown of mean mass concentrations of trace elements characterized through XRF in $PM_{2.5}$ at SPARTAN sites. Mass concentrations of each element are reported in ng/m^3. Total $PM_{2.5}$ mass concentrations are reported in µg/m^3. Sites are reported in alphabetical order. Elemental mean concentrations recorded as "n/a" indicates no sampled data above the elemental acceptance limit.

	PM2.5	Al	Si	S	Cl	K	Ca	Ti	V	Fe	Zn	Ce
Abu Dhabi	38.61	562.9	1603.0	3944.0	37.2	271.0	1067.2	36.5	8.5	397.2	38.8	3.7
Bandung	36.66	80.0	112.5	846.8	25.4	271.7	35.4	6.3	0.5	36.8	20.5	3.0
Beijing	24.03	133.3	301.4	1170.9	9.8	157.8	116.0	42.7	0.2	192.9	33.9	18.8
Dhaka	123.19	122.0	431.4	323.9	224.0	193.2	96.0	6.9	0.5	78.4	454.5	0.9
Halifax	3.06	5.1	3.6	24.5	13.8	3.6	1.4	n/a	0.0	1.5	0.5	0.2
Hanoi	28.19	221.3	598.2	1861.1	111.9	474.6	161.6	15.4	1.9	195.9	451.8	1.8
Ilorin	39.76	222.7	578.5	229.3	17.7	145.8	75.5	22.4	0.7	131.8	53.5	1.5
Lethbridge	5.04	82.9	123.7	236.3	n/a	42.5	42.9	n/a	0.3	28.3	2.8	1.2
Rehovot	13.01	97.1	235.4	795.8	9.8	81.6	83.6	10.8	2.3	72.9	8.1	0.4
Seoul	21.18	219.0	554.0	2061.1	26.5	268.4	107.2	22.3	5.7	260.7	52.4	2.7
Sherbrooke	4.86	21.9	45.3	142.1	1.2	28.1	11.4	12.1	0.1	19.6	2.4	0.3
Singapore	23.93	72.4	131.6	1357.9	39.3	294.6	51.3	113.5	19.5	56.2	94.3	25.1
Toronto	6.45	41.2	91.7	403.0	n/a	51.8	71.6	n/a	0.4	86.5	17.9	2.1

	Pb	As	Co	Cr	Cu	Mg	Mn	Ni	Rb	Sr	Se
Abu Dhabi	3.9	1.2	1.3	2.1	4.3	412.0	8.5	3.3	2.7	16.8	0.9
Bandung	8.3	1.3	0.3	1.6	7.3	39.9	1.1	1.2	1.7	n/a	0.2
Beijing	5.4	2.5	0.2	1.1	1.3	64.2	11.3	0.2	0.3	0.5	1.1
Dhaka	462.5	10.7	1.0	0.8	3.9	33.5	9.5	0.8	1.8	0.9	0.9
Halifax	n/a	0.1	n/a	0.2	0.5	3.4	0.1	0.1	n/a	n/a	0.0
Hanoi	121.6	8.3	1.0	1.9	10.7	84.5	31.0	1.5	3.4	n/a	1.4
Ilorin	6.3	0.4	0.6	0.6	0.9	30.8	4.0	0.2	0.7	1.4	0.1
Lethbridge	n/a	0.6	n/a	3.3	n/a	21.3	0.8	n/a	n/a	n/a	0.4
Rehovot	2.2	0.7	0.4	1.0	2.8	47.8	1.4	1.4	n/a	0.4	0.3
Seoul	12.2	3.5	0.7	3.4	10.9	89.8	11.8	2.8	n/a	n/a	1.6
Sherbrooke	0.2	0.4	n/a	0.3	1.1	6.2	0.8	0.1	n/a	n/a	0.1
Singapore	7.6	2.1	2.0	4.4	2.0	46.3	4.7	5.0	n/a	n/a	0.8
Toronto	10.2	0.8	0.4	1.2	3.6	25.4	2.7	0.5	n/a	n/a	0.5

4.3 CRUSTAL EFS FOR XRF RESULTS

The enrichment factors (EFs) for trace elements at each of the SPARTAN sites were calculated using the XRF-measured trace element concentrations in Eq. 4.3 below (previously detailed in section 2.2), and are shown in Figure 4.3:

$$EF_{X,2.5} = \frac{[X/Fe]_{PM_{2.5}}}{[X/Fe]_{Taylor}} \quad \text{Eq. 4.3}$$

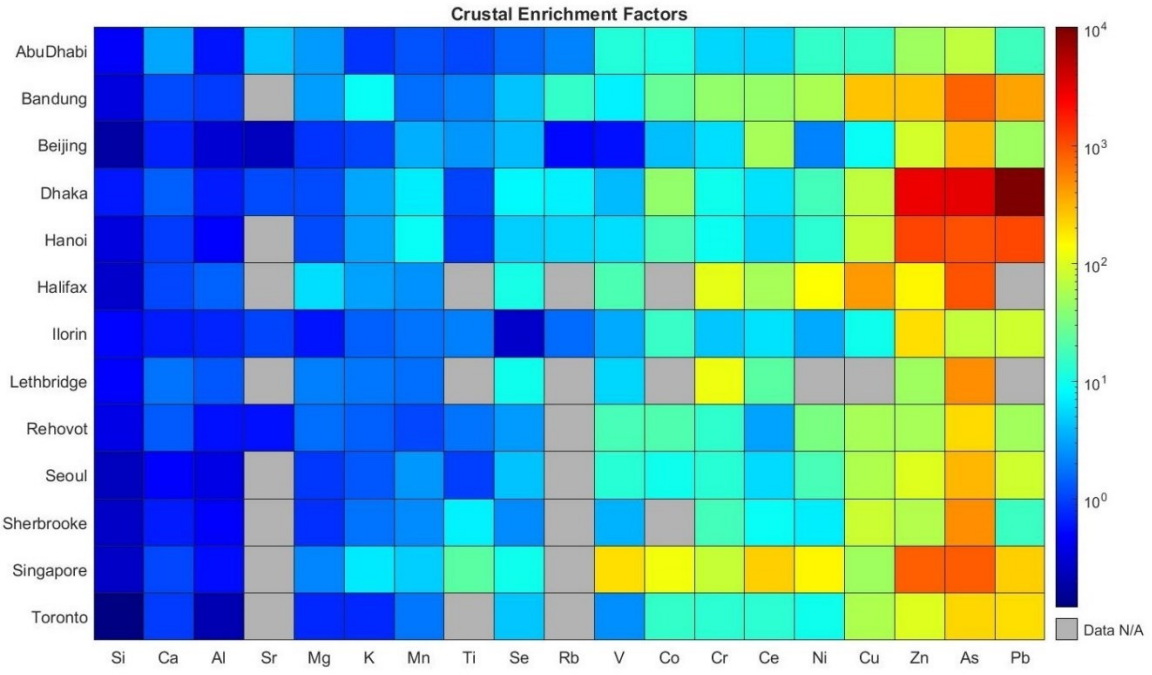

Figure 4.3: Crustal enrichment factors (EF) for XRF-measured trace metal $PM_{2.5}$ relative to crustal ratios of the given element and iron (Eq. 2.1). Elements are sorted by mean enrichment factor across all sites; sites are listed alphabetically. Grey squares indicate all measured concentrations were below elemental acceptance limit at that site.

Elements in the figure are sorted by mean enrichment factor across all sites, with those having the lowest mean EF values on the left and those with increasing mean EF values to the right. This can offer some perspective into which elements are generally enriched at

SPARTAN sites compared to crustal concentrations. Elements classified at both the high-end (anthropogenic) and low-end (crustal or "natural") are consistent with their typical natures, providing confidence for the results in Figure 4.3. As seen above, elements typically considered crustal are those with the lowest EFs; Si, Sr, Al, Ca, Mg, Ti, Rb, K, Mn, Se, and Co all have mean EF values below 10, indicating their relatively low enrichment in ambient $PM_{2.5}$. On the other end of the spectrum, the most heavily enriched elements in the sampled $PM_{2.5}$ are Pb, As, and Zn. These metals have mean EF values over 100, indicating largely anthropogenic sources, which is consistent with their nature as anthropogenically-emitted metals in $PM_{2.5}$.

In general, SPARTAN sites with higher levels of ambient $PM_{2.5}$ typically see higher enrichments of anthropogenically emitted metals, with As, Pb, and Zn commonly elevated. This can be seen in the Hanoi and Dhaka sites, where EF values for As, Pb, and Zn are all ~1,000, some of the highest enrichments observed. Dhaka has the highest EF of any SPARTAN site, as it exhibited a Pb EF value over 10,000 – previous issues with Dhaka and Pb have been discussed in section 3.3. The continued presence of extremely high levels of Pb in ambient particulate matter in Dhaka is cause for serious health concerns, and further assessment of this aspect of the site is crucial to ensuring those concerns are addressed in the future.

The reverse relationship between PM and EFs is also shown, as some of the SPARTAN sites with the lowest typical concentrations of $PM_{2.5}$ see very few notable enrichments – three of the four Canadian sites in particular see EF values over 100 only for As, the metal with the second highest network-wide mean EF of all elements measured. This is consistent

with the characterization of these sites as low-PM environments in a country with strict air quality guidelines. SPARTAN sites in arid regions (Abu Dhabi, Ilorin) also show few notable enrichments, which may be due in part to the large quantities of Fe (and other crustal elements) in windswept dust that can mask anthropogenic enrichment of non-crustal elements.

Beijing is notable in this investigation especially in comparison to EF values determined previously in Chapter 3, where enrichment in As, Pb, and Se were apparent and determined to stem primarily from the coal-burning in the region. From XRF, these metals are not significantly enriched in comparison to other SPARTAN sites, indicating that the sources of these metals in $PM_{2.5}$ have been diminished in some capacity. This is potentially a success story for Beijing and China generally, as the country implemented a clean air policy in 2013 that led to major changes in the coal industry. Beijing specifically shut down all four of its coal-fired power plants from 2014-2017, and switched roughly 4.8 million households in the surrounding area from coal heating to natural gas and electricity in 2017. Atmospheric modelling has shown that these measures have been effective in reducing $PM_{2.5}$ in the country[99], and as these XRF results are the first SPARTAN samples to be characterized from the site since the end of 2017, it appears the changes have also made an appreciable difference on trace metal $PM_{2.5}$ in the city.

Also notable from this exploration is the Singapore site, which has been previously described in section 3.5 based on its unique properties. To briefly reiterate, the proximity of the site to the bustling Port of Singapore and to petroleum refineries is likely driving enhancements of anthropogenically sourced trace metals such as nickel, cerium, zinc,

arsenic, and notably vanadium (V). These enhancements can be clearly seen in Figure 4.3, with nickel and vanadium levels in particular notably above other SPARTAN sites. The enhancement of nickel seen through XRF gives further credence to the importance of petroleum on ambient PM in Singapore, as V and Ni are the two most abundant metals in petroleum.[100] This impact can also be seen in the relatively low enhancement of Pb at the site due to Singapore's widespread use of petroleum in lieu of coal-burning, as coal combustion is one of the most common sources of ambient lead $PM_{2.5}$.

4.4 COMPARISONS TO ICP-MS RESULTS

4.4.1 XRF-Measured Arsenic $PM_{2.5}$ at SPARTAN Sites

In continuing the elemental analysis of the ambient $PM_{2.5}$ at SPARTAN sites, specific attention was paid to previously discussed trace metals arsenic (As) and lead (Pb) for their potential health concerns. Mass concentrations of As measured through XRF at SPARTAN sites are shown in Figure 4.4, along with the excess lifetime risk of cancer thresholds of 6.6 ng/m^3 (1:100,000) and 0.66 ng/m^3 (1:1,000,000).

As mentioned, some sites had no XRF data available at the time of analysis, including the Kanpur site which demonstrated the highest quantity of As $PM_{2.5}$ in the ICP-MS based analysis. Comparing the remaining sites however, it can be seen that Dhaka now shows the highest levels of As $PM_{2.5}$ among all SPARTAN sites, increasing from ~6 ng/m^3 to roughly 10.7 ng/m^3, jumping by approximately 78%. This further amplifies the need to address trace

metal $PM_{2.5}$ in the region, as these higher levels of As may contribute to cancer and other negative health impacts for those living in the Dhaka region.

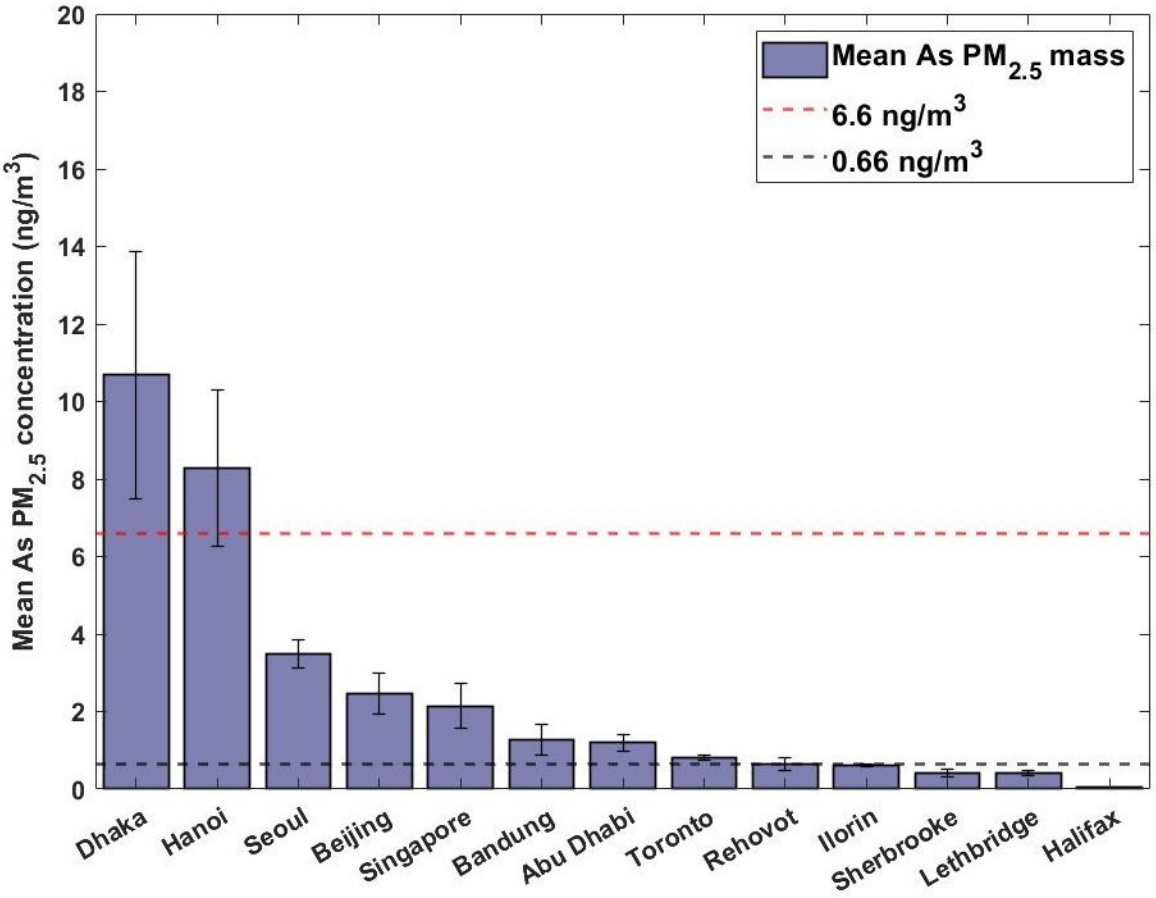

Figure 4.4: Concentrations of As measured by XRF in $PM_{2.5}$ samples taken from SPARTAN sites, with standard error bars shown. Dotted red line represents 1:100,000 excess lifetime risk of cancer due to As exposure (6.6 ng/m^3). Dotted black line represents 1:1,000,000 excess lifetime risk of cancer due to arsenic exposure (0.66 ng/m^3).

The Hanoi site exhibits similar levels of arsenic trace metal PM as observed through ICP-MS (roughly 8 ng/m^3), indicating that emissions of As continue to be a health concern in the area. Sites located in Canada generally have low levels of ambient As $PM_{2.5}$ as seen previously, with Lethbridge, Halifax, Toronto, and Sherbrooke exhibiting As $PM_{2.5}$ mass concentrations under 1 ng/m^3. Ilorin and Rehovot were the only two international sites

sampled to also fall under this mark, which aligns with their lower population densities. The Beijing site continues to show improvements in air quality especially in relation to trace metal $PM_{2.5}$, as arsenic mass concentrations recorded over the XRF analysis period were significantly lower than the 6.6 ng/m^3 exposure threshold that was previously exceeded.

Among sites with only XRF data, Seoul exhibits a moderate concentration of As $PM_{2.5}$ (approximately 3.5 ng/m^3) that bears further observation, but is not of immediate concern. The site in Abu Dhabi shows relatively low concentrations of arsenic compared to most international SPARTAN sites at ~1.2 ng/m^3, indicating that the trace metal is not of significant concern in the region.

4.4.2 XRF-Measured Lead $PM_{2.5}$ at SPARTAN Sites

Levels of lead detected in $PM_{2.5}$ samples were generally lower than previous ICP-MS analysis, with only two SPARTAN sites exhibiting mean Pb $PM_{2.5}$ concentrations above 15 ng/m^3, and only one site measuring over the 150 ng/m^3 US NAAQS threshold discussed previously (Dhaka, 463 ng/m^3). The factors influencing the high levels of lead $PM_{2.5}$ specifically in Dhaka have been discussed previously, with additional contributions stemming from lead-acid battery manufacturing and recycling in the region, similarly to the Bandung site discussed in Section 3.5. It should be noted that this level is three times the recommended maximum 3-month mean concentration of total suspended Pb particles by US authorities, and as such is a serious health concern for residents of the area. These health risks are greatest for children, as lead is a neurotoxin that can negatively impact healthy development and cause serious long-term effects on children if significantly

exposed to Pb. An analysis of the potential for lead exposure among children (ages 2-3) in Bangladesh near Dhaka found that total suspended lead particles in the region reached a mean value of 1220 ng/m^3, nearly ten times the US standard and over twice the WHO guideline of 500 ng/m^3 annual mean Pb concentration.[101] The observed mean Pb $PM_{2.5}$ concentration at the Dhaka site of 463 ng/m^3 would align with these levels of Pb TSP.

The only other SPARTAN site analyzed here with a significant concentration of Pb in $PM_{2.5}$ is the Hanoi site, which has a similar mean concentration as previous ICP-MS analysis (122 ng/m^3 vs 141 ng/m^3). This is a slight improvement, but still bears monitoring at the Hanoi site in the future as it hovers near the 150 ng/m^3 mark as this may be a product of temporal sampling differences. The Kanpur site which previously exhibited high levels of lead in ambient particulate matter was not analyzed through XRF as of the time of publication of this work, but is another site that merits observation in the future in relation to Pb $PM_{2.5}$.

Improvements in lead concentrations were observed at the Bandung (34.6 ng/m^3 vs 8.3 ng/m^3) and Beijing (41.3 ng/m^3 to 5.4 ng/m^3), which is a positive indication for air quality and community health in those areas. The site in Beijing in particular continues to exhibit improvements across the board in air quality, which is likely linked to the previously discussed policy change in the region from coal combustion to natural gas and electricity which was made effective in late 2017. This impact on Pb specifically is another indicator that the elimination of coal burning has improved ambient PM, as lead $PM_{2.5}$ is a common marker for coal combustion, and a roughly 87% decrease in the Pb mass concentrations suggests far less contribution from those combustion sources.

5 CONCLUSION

5.1 FUTURE WORK AND IMPROVEMENTS

This work illustrates both the tremendous work that has been done by the entire SPARTAN team, from researchers to principal investigators to collaborators on the ground at SPARTAN sampling sites, as well as the future potential for the network. There are several avenues for future development for SPARTAN that will serve to increase understanding of ambient particulate matter globally. These include new site introduction, further honing lab analysis as well as utilizing additional analysis techniques to obtain more detailed information, and integrating complementary chemical transport modelling to fill in temporal and spatial gaps in SPARTAN coverage.

SPARTAN continues to expand its network coverage across the globe, with new sites currently in development in South America (Santiago, Chile; Palmira, Colombia), and an additional seven sites to sample in collaboration with the MAIA (Multi-Angle Imager for Aerosols) project led by NASA in the near future. These sites are located across the world, from North America (Pasadena, California, USA) to Africa (Addis Ababa, Ethiopia; Johannesburg, South Africa) to Asia (Delhi, India; Haifa, Israel; Kaohsiung, Taiwan; Taipei, Taiwan). These additional sampling locations will allow for deeper investigations of regions with historical data (India, Israel, South Africa) and also provide new regions of interest. Collaboration with NASA will also spur method and analysis development in order to obtain the maximum information possible from the sampled filters of this project.

The methodologies used in the SPARTAN laboratory are extensive and robust, but development of analysis both new and current is key to ensuring that as much information as possible can be successfully obtained from the limited numbers of filters that are sampled at SPARTAN sites. In relation to this work specifically, incorporation of X-ray fluorescence into the SPARTAN network is still in its relative infancy in comparison to other analysis techniques, and as such will continue to develop in the future. One such development will be to compare directly between results obtained from XRF and from ICP-MS for the same samples, allowing a more accurate comparison of the SPARTAN methodologies. This could also potentially be used to retroactively examine earlier samples and put them more precisely in context with current and future results, even with methodology changes.

Some of these methodology changes involve implementing new analysis methods, allowing new information to be captured to further increase understanding of ambient particulate matter. SPARTAN is collaborating with the IMPROVE group at the University of California, Davis in order to use FTIR (Fourier Transform Infrared Spectroscopy) analysis as well as HIPS (Hybrid integrating plate/sphere) analysis to obtain organic carbon/elemental carbon and black carbon data, respectively. An additional collaboration with Dr. Rajan Chakrabarty at Washington University in St. Louis is implementing UV-Vis spectroscopy for characterization of brown carbon. Finally, AMS (aerosol mass spectrometry) analysis is also in development in the SPARTAN laboratory with the aim of characterizing organic compounds in $PM_{2.5}$ sampled from ground sites. These new analysis techniques can provide a greater picture of the nature of $PM_{2.5}$ at SPARTAN locations alongside the techniques used to date.

As implementation of new methods of analysis occurs, further contextualization of the results through reporting of metrics of interest is key. This includes further characterizing uncertainties in SPARTAN especially as new analytical methods are incorporated into operations, exploring new means of reporting data, and further enhancing the robustness of the data collected. In future, additional collocated sampling investigations would offer insight into the total uncertainties associated with new SPARTAN operations like XRF analysis and others. This is especially useful due to the number of independent factors that can influence observed concentrations, like the temporality and seasonality of sampling, wind impact, and the variability of emissions in the region. Further collocated sampling would reduce the impact of these factors and allow for elemental uncertainties to be established for XRF and other analysis methods.

Additional lab analysis is not the only avenue for further exploring ambient particulate matter at SPARTAN locations, as recent developments in chemical transport modelling offer the ability to examine modelled concentrations versus their real-world counterparts. This work has the potential to be used in complement with chemical transport modelling through the GEOS-Chem High Performance (GCHP) global model, which could further illuminate differences between instantaneous sampling and the 9-day rolling sampling protocol of the SPARTAN network. The ability of SPARTAN to provide real samples for the model to compare against is helpful for both network and model in order to discover the sources of discrepancies or validate results.

In addition to further analysis improvements, there is also the potential for greater collection of data as SPARTAN continues operations, especially in light of many sites

ceasing or delaying sampling due to the COVID-19 pandemic. As sites return to normal operations, long-term trends and seasonal variances can be determined for a greater number of sites, leading to more local and regional data. Expansion of both the network and the analytical methods used in SPARTAN will provide valuable information on the nature of global particulate matter in addition to the findings presented in this work.

5.2 Interpretation of Results

Globally consistent measurements of airborne metal concentrations in $PM_{2.5}$ are essential to assessing and understanding the variations in ambient particulate matter across the world. Over 1000 samples of fine particulate matter ($PM_{2.5}$) from 21 unique sampling sites located across four continents were collected and analyzed through SPARTAN, with concentrations of 15 different trace metals reported by ICP-MS analysis and 22 unique elements reported through XRF analysis. As the SPARTAN network continues to develop, these sampling protocols will continue to be improved to better report the chemical composition of trace metals in $PM_{2.5}$.

In general, it was found that several elements were enriched compared to their concentrations in the crust – in particular, elements such as Pb, As, and Zn that have anthropogenic sources were greatly enriched in sampled $PM_{2.5}$. This enrichment was most notable in large, densely populated urban areas such as Beijing, Dhaka, Kanpur, and Hanoi, but was seen generally across many SPARTAN sites. It has been previously shown that anthropogenic dust (including fugitive, industry and combustion sources) can contribute up to 10% of $PM_{2.5}$, and includes trace metals that can have adverse health effects.[26]

The enrichment of potentially harmful elements in fine particulate matter from anthropogenic sources is of global relevance to public health and warrants further attention. For example, we found in Dhaka and Kanpur that Pb concentrations exceeded the US National Ambient Air Quality three-month guideline of 150 ng/m^3, and that concentrations of the carcinogen As approached or exceeded the World Health Organization's 1:100,000 excess lifetime risk level (6.6 ng/m^3) in Kanpur, Hanoi, Dhaka, and historically in Beijing. Other sites saw particularly high levels of specific trace metals that were anthropogenically influenced, and which may be linked to certain industries in those sites – for example, high V concentrations in Singapore where shipping fuel burning is prevalent, as well as Ni concentrations showing enrichment in areas where fuel burning is dominant.

More generally, the high concentrations of several potentially harmful elements (e.g. Zn, Pb, Cd, Se, and As) at densely populated cities such as Dhaka, Kanpur, and Hanoi motivate measurements to understand and better control emissions in large cities worldwide. Evidence of the impact of air quality regulation can be seen at the Beijing site, which demonstrated high trace metal $PM_{2.5}$ before elimination of coal-burning took place in late 2017. The Beijing site showed marked improvements in the overall mass concentrations of $PM_{2.5}$ sampled, as well as in reducing the quantity of harmful trace metals such as lead in $PM_{2.5}$ after these changes were implemented. The near-immediate impact of the policy change in the Beijing region should provide confidence that tackling $PM_{2.5}$ emissions at the source can be effective.

The SPARTAN project is currently expanding its reach by beginning measurements in a greater diversity of cities in order to better capture the current state of air quality in more

of the world's developing cities. These results relating to trace metal quantity, enrichment and relative abundance display the potential for expanded sampling into new, geographically diverse regions, and illustrates how cities and their inhabitants in these regions can be exposed to potentially hazardous levels of trace metal $PM_{2.5}$ on an everyday basis. Levels of toxic metal content in $PM_{2.5}$ showed varied levels of enrichment based on anthropogenic activities, and these measurements provide a strong foundation to better understand the potential adverse human health impacts of these metals worldwide.

**Note: some material for this Chapter has been adapted from "Large Global Variations in Measured Airborne Metal Concentrations Driven by Anthropogenic Sources" by Jacob McNeill et. al, published in* Scientific Reports *(December 2020)*

REFERENCES

(1) Stanaway, J. D.; Afshin, A.; Gakidou, E.; Lim, S. S.; Abate, D.; Hassen Abate, K.; Abbafati, C.; Abbasi, N.; Abbastabar, H.; Abd-Allah, F.; et al. *Global, Regional, and National Comparative Risk Assessment of 84 Behavioural, Environmental and Occupational, and Metabolic Risks or Clusters of Risks for 195 Countries and Territories, 1990â€“2017: A Systematic Analysis for the Global Burden of Disease Study 2017*; 2018; Vol. 392. https://doi.org/10.1016/S0140-6736(18)32225-6.

(2) Martin, R. V.; Brauer, M.; van Donkelaar, A.; Shaddick, G.; Narain, U.; Dey, S. No One Knows Which City Has the Highest Concentration of Fine Particulate Matter. *Atmos. Environ. X* **2019**, *3*. https://doi.org/10.1016/j.aeaoa.2019.100040.

(3) Lippmann, M. Toxicological and Epidemiological Studies of Cardiovascular Effects of Ambient Air Fine Particulate Matter (PM2.5) and Its Chemical Components: Coherence and Public Health Implications. *Crit. Rev. Toxicol.* **2014**, *44* (4), 299–347. https://doi.org/10.3109/10408444.2013.861796.

(4) Gent, J. F.; Koutrakis, P.; Belanger, K.; Triche, E.; Holford, T. R.; Bracken, M. B.; Leaderer, B. P. Symptoms and Medication Use in Children with Asthma and Traffic-Related Sources of Fine Particle Pollution. *Environ. Health Perspect.* **2009**, *117* (7), 1168–1174. https://doi.org/10.1289/ehp.0800335.

(5) Kampa, M.; Castanas, E. Human Health Effects of Air Pollution. *Environ. Pollut.* **2008**, *151* (2), 362–367. https://doi.org/http://dx.doi.org/10.1016/j.envpol.2007.06.012.

(6) Shuster-Meiseles, T.; Shafer, M. M.; Heo, J.; Pardo, M.; Antkiewicz, D. S.; Schauer, J. J.; Rudich, A.; Rudich, Y. ROS-Generating/ARE-Activating Capacity of Metals in Roadway Particulate Matter Deposited in Urban Environment. *Environ. Res.* **2016**, *146*, 252–262. https://doi.org/http://dx.doi.org/10.1016/j.envres.2016.01.009.

(7) Rajagopalan, S.; Brook, R. D. Air Pollution and Type 2 Diabetes: Mechanistic Insights. *Diabetes* **2012**, *61* (12), 3037–3045. https://doi.org/10.2337/db12-0190.

(8) US EPA, O. Particulate Matter (PM) Basics https://www.epa.gov/pm-pollution/particulate-matter-pm-basics (accessed Jan 25, 2021).

(9) Liang, C. S.; Duan, F. K.; He, K. Bin; Ma, Y. L. Review on Recent Progress in Observations, Source Identifications and Countermeasures of PM2.5. *Environment International*. Elsevier Ltd January 1, 2016, pp 150–170. https://doi.org/10.1016/j.envint.2015.10.016.

(10) Malm, W. C.; Sisler, J. F.; Huffman, D.; Eldred, R. A.; Cahill, T. A. Spatial and Seasonal Trends in Particle Concentration and Optical Extinction in the United States. *J. Geophys. Res.* **1994**, *99* (D1), 1347–1370. https://doi.org/10.1029/93JD02916.

(11) O'Brien, R. E.; Ridley, K. J.; Canagaratna, M. R.; Jayne, J. T.; Croteau, P. L.; Worsnop, D. R.; Hapsari Budisulistiorini, S.; Surratt, J. D.; Follett, C. L.; Repeta, D. J.; et al. Ultrasonic Nebulization for the Elemental Analysis of Microgram-Level Samples with Offline Aerosol Mass Spectrometry. *Atmos. Meas. Tech.* **2019**, *12* (3), 1659–1671. https://doi.org/10.5194/amt-12-1659-2019.

(12) Coury, C.; Dillner, A. M. A Method to Quantify Organic Functional Groups and Inorganic Compounds in Ambient Aerosols Using Attenuated Total Reflectance FTIR Spectroscopy and Multivariate Chemometric Techniques. *Atmos. Environ.* **2008**, *42* (23), 5923–5932. https://doi.org/10.1016/j.atmosenv.2008.03.026.

(13) Pandey, P.; Patel, D. K.; Khan, A. H.; Barman, S. C.; Murthy, R. C.; Kisku, G. C. Temporal Distribution of Fine Particulates ($PM_{2.5,}$ PM_{10}), Potentially Toxic Metals, PAHs and Metal-Bound Carcinogenic Risk in the Population of Lucknow City, India. *J. Environ. Sci. Heal. Part A* **2013**, *48* (7), 730–745. https://doi.org/10.1080/10934529.2013.744613.

(14) Zeng, X.; Xu, X.; Zheng, X.; Reponen, T.; Chen, A.; Huo, X. Heavy Metals in PM2.5 and in Blood, and Children's Respiratory Symptoms and Asthma from an e-Waste Recycling Area. *Environ. Pollut.* **2016**, *210*, 346–353. https://doi.org/10.1016/j.envpol.2016.01.025.

(15) Hartono, D.; Lioe, B.; Zhang, Y.; Li, B.; Yu, J. Impacts of Particulate Matter (PM2.5) on the Behavior of Freshwater Snail Parafossarulus Striatulus. *Sci. Rep.* **2017**, *7* (1), 1–8. https://doi.org/10.1038/s41598-017-00449-5.

(16) Zhao, P.; Lu, W.; Hong, Y.; Chen, J.; Dong, S.; Huang, Q. Long-Term Wet Precipitation of PM2.5 Disturbed the Gut Microbiome and Inhibited the Growth of Marine Medaka Oryzias Melastigma. *Sci. Total Environ.* **2021**, *755*, 142512. https://doi.org/10.1016/j.scitotenv.2020.142512.

(17) Rai, P. K. Impacts of Particulate Matter Pollution on Plants: Implications for Environmental Biomonitoring. *Ecotoxicology and Environmental Safety*. Academic Press July 1, 2016, pp 120–136. https://doi.org/10.1016/j.ecoenv.2016.03.012.

(18) Dockery, D. W.; Pope, C. A.; Xu, X.; Spengler, J. D.; Ware, J. H.; Fay, M. E.; Ferris, B. G.; Speizer, F. E. An Association between Air Pollution and Mortality in Six U.S. Cities. *N. Engl. J. Med.* **1993**, *329* (24), 1753–1759. https://doi.org/10.1056/nejm199312093292401.

(19) Pope, C. A.; Burnett, R. T.; Thun, M. J.; Calle, E. E.; Krewski, D.; Ito, K.; Thurston, G. D. Lung Cancer, Cardiopulmonary Mortality, and Long-Term Exposure to Fine Particulate Air Pollution. *J. Am. Med. Assoc.* **2002**, *287* (9), 1132–1141. https://doi.org/10.1001/jama.287.9.1132.

(20) Bell, M. L.; Ebisu, K.; Leaderer, B. P.; Gent, J. F.; Lee, H. J.; Koutrakis, P.; Wang, Y.; Dominici, F.; Peng, R. D. Associations of PM2.5 Constituents and Sources with Hospital Admissions: Analysis of Four Counties in Connecticut and Massachusetts (USA) for Persons ≥ 65 Years of Age. *Environ. Health Perspect.* **2014**, *122* (2), 138–144. https://doi.org/10.1289/ehp.1306656.

(21) Song, C.; He, J.; Wu, L.; Jin, T.; Chen, X.; Li, R.; Ren, P.; Zhang, L.; Mao, H. Health Burden Attributable to Ambient PM2.5 in China. *Environ. Pollut.* **2017**, *223*, 575–586. https://doi.org/10.1016/j.envpol.2017.01.060.

(22) West, J. J.; Cohen, A.; Dentener, F.; Brunekreef, B.; Zhu, T.; Armstrong, B.; Bell, M. L.; Brauer, M.; Carmichael, G.; Costa, D. L.; et al. "What We Breathe Impacts Our Health: Improving Understanding of the Link between Air Pollution and Health." *Environ. Sci. Technol.* **2016**, *50* (10), 4895–4904. https://doi.org/10.1021/acs.est.5b03827.

(23) Wu, X.; Nethery, R. C.; Sabath, M. B.; Braun, D.; Dominici, F. Air Pollution and COVID-19 Mortality in the United States: Strengths and Limitations of an Ecological Regression Analysis. *Sci. Adv.* **2020**, *6* (45), eabd4049. https://doi.org/10.1126/SCIADV.ABD4049.

(24) Frontera, A.; Cianfanelli, L.; Vlachos, K.; Landoni, G.; Cremona, G. Severe Air Pollution Links to Higher Mortality in COVID-19 Patients: The "Double-Hit" Hypothesis. *J. Infect.* **2020**, *81* (2), 255–259. https://doi.org/10.1016/j.jinf.2020.05.031.

(25) Holben, B. N.; Eck, T. F.; Slutsker, I.; Tanré, D.; Buis, J. P.; Setzer, A.; Vermote, E.; Reagan, J. A.; Kaufman, Y. J.; Nakajima, T.; et al. AERONET - A Federated Instrument Network and Data Archive for Aerosol Characterization. *Remote Sens. Environ.* **1998**, *66* (1), 1–16. https://doi.org/10.1016/S0034-4257(98)00031-5.

(26) Philip, S.; Martin, R. V; Snider, G.; Weagle, C. L.; van Donkelaar, A.; Brauer, M.; Henze, D. K.; Kilmont, Z.; Venkataraman, C.; Guttikunda, S. K.; et al. Anthropogenic Fugitive, Combustion and Industrial Dust Is a Significant, Underrepresented Fine Particulate Matter Source in Global Atmospheric Models. *Environ. Res. Lett.* **2017**, *12* (044018). https://doi.org/10.1088/1748-9326/aa65a4.

(27) Weagle, C. L.; Snider, G.; Li, C.; Van Donkelaar, A.; Philip, S.; Bissonnette, P.; Burke, J.; Jackson, J.; Latimer, R.; Stone, E.; et al. Global Sources of Fine Particulate Matter: Interpretation of PM2.5 Chemical Composition Observed by SPARTAN Using a Global Chemical Transport Model. *Environ. Sci. Technol.* **2018**, *52* (20), 11670–11681. https://doi.org/10.1021/acs.est.8b01658.

(28) Brauer, M.; Brook, J. R.; Chu, Y. L.; Christidis, T.; Crouse, D. L.; Erickson, A.; Hystad, P.; Li, C.; Martin, R. V.; Meng, J.; et al. MAPLE: Mortality-Air Pollution Associations in Low Exposure Environments; 2019 HEI Conference, 2019.

(29) University, C. for I. E. S. I. N.-C.-C. Gridded Population of the World, Version 4 (GPWv4): Population Count. NASA Socioeconomic Data and Applications Center (SEDAC): Palisades, NY 2016.

(30) World Urbanization Prospects - Population Division - United Nations https://population.un.org/wup/Publications/ (accessed Dec 9, 2019).

(31) Snider, G.; Weagle, C. L.; Martin, R. V.; van Donkelaar, A.; Conrad, K.; Cunningham, D.; Gordon, C.; Zwicker, M.; Akoshile, C.; Artaxo, P.; et al. SPARTAN: A Global Network to Evaluate and Enhance Satellite-Based Estimates of Ground-Level Particulate Matter for Global Health Applications. *Atmos. Meas. Tech.* **2015**, *8* (1), 505–521. https://doi.org/10.5194/amt-8-505-2015.

(32) Chen, S.; Wang, X.; Niu, Y.; Sun, P.; Duan, M.; Xiao, Y.; Guo, P.; Gong, H.; Wang, G.; Xue, Q. Simple and Cost-Effective Methods for Precise Analysis of Trace Element Abundances in Geological Materials with ICP-MS. *Sci. Bull.* **2017**, *62* (4), 277–289. https://doi.org/10.1016/j.scib.2017.01.004.

(33) Wang, H.; He, M.; Chen, B.; Hu, B. Advances in ICP-MS-Based Techniques for Trace Elements and Their Species Analysis in Cells. *Journal of Analytical Atomic Spectrometry*. Royal Society of Chemistry September 1, 2017, pp 1650–1659. https://doi.org/10.1039/c6ja00414h.

(34) Lo Dico, G. M.; Galvano, F.; Dugo, G.; D'ascenzi, C.; Macaluso, A.; Vella, A.; Giangrosso, G.; Cammilleri, G.; Ferrantelli, V. Toxic Metal Levels in Cocoa Powder and Chocolate by ICP-MS Method after Microwave-Assisted Digestion. *Food Chem.* **2018**, *245*, 1163–1168. https://doi.org/10.1016/j.foodchem.2017.11.052.

(35) Wilschefski, S.; Baxter, M. Inductively Coupled Plasma Mass Spectrometry: Introduction to Analytical Aspects. *Clin. Biochem. Rev.* **2019**, *40* (3), 115–133. https://doi.org/10.33176/aacb-19-00024.

(36) Roje, V. Multi-Elemental Analysis of Marine Sediment Reference Material MESS-3: One-Step Microwave Digestion and Determination by High Resolution Inductively Coupled Plasma-Mass Spectrometry (HR-ICP-MS). *Chem. Pap.* **2010**, *64* (4), 409–414. https://doi.org/10.2478/s11696-010-0022-x.

(37) Enamorado-Báez, S. M.; Abril, J. M.; Gómez-Guzmán, J. M. Determination of 25 Trace Element Concentrations in Biological Reference Materials by ICP-MS Following Different Microwave-Assisted Acid Digestion Methods Based on Scaling Masses of Digested Samples. *ISRN Anal. Chem.* **2013**, *2013*, 1–14. https://doi.org/10.1155/2013/851713.

(38) Garcia-Aleix, J. R.; Delgado-Saborit, J. M.; Verdú-Martin, G.; Amigó-Descarrega, J. M.; Esteve-Cano, V. Trends in Arsenic Levels in PM10 and PM2.5 Aerosol Fractions in an Industrialized Area. *Environ. Sci. Pollut. Res.* **2013**, *21* (1), 695–703. https://doi.org/10.1007/s11356-013-1950-0.

(39) Islam, M. F.; Majumder, S. S.; Mamun, A. Al; Khan, M. B.; Rahman, M. A.; Salam, A. Trace Metals Concentrations at the Atmosphere Particulate Matters in the Southeast Asian Mega City (Dhaka, Bangladesh). *Open J. Air Pollut.* **2015**, *04* (02), 86–98. https://doi.org/10.4236/ojap.2015.42009.

(40) Kulkarni, P.; Chellam, S.; Flanagan, J. B.; Jayanty, R. K. M. Microwave Digestion—ICP-MS for Elemental Analysis in Ambient Airborne Fine Particulate Matter: Rare Earth Elements and Validation Using a Filter Borne Fine Particle Certified Reference Material. *Anal. Chim. Acta* **2007**, *599* (2), 170–176. https://doi.org/10.1016/J.ACA.2007.08.014.

(41) Jenkins, R.; Manne, R.; Robin, R.; Senemaud, C. IUPAC—Nomenclature System for x-Ray Spectroscopy. *X-Ray Spectrom.* **1991**, *20* (3), 149–155. https://doi.org/10.1002/xrs.1300200308.

(42) Brouwer, P. *THEORY OF XRF Getting Acquainted with the Principles*; 2003.

(43) Indresand, H.; Dillner, A. M. Experimental Characterization of Sulfur Interference in IMPROVE Aluminum and Silicon XRF Data. *Atmos. Environ.* **2012**, *61*, 140–147. https://doi.org/10.1016/j.atmosenv.2012.06.079.

(44) Brauer, M.; Freedman, G.; Frostad, J.; van Donkelaar, A.; Martin, R. V; Dentener, F.; Dingenen, R. van; Estep, K.; Amini, H.; Apte, J. S.; et al. Ambient Air Pollution Exposure Estimation for the Global Burden of Disease 2013. *Environ. Sci. Technol.* **2015**. https://doi.org/10.1021/acs.est.5b03709.

(45) van Donkelaar, A.; Martin, R. V; Brauer, M.; Hsu, N. C.; Kahn, R. A.; Levy, R. C.; Lyapustin, A.; Sayer, A. M.; Winker, D. M. Global Estimates of Fine Particulate Matter Using a Combined Geophysical-Statistical Method with Information from Satellites, Models, and Monitors. *Environ. Sci. Technol.* **2016**, *50* (7), 3762–3772. https://doi.org/10.1021/acs.est.5b05833.

(46) Cohen, A. J.; Brauer, M.; Burnett, R.; Anderson, H. R.; Frostad, J.; Estep, K.; Balakrishnan, K.; Brunekreef, B.; Dandona, L.; Dandona, R.; et al. Estimates and 25-Year Trends of the Global Burden of Disease Attributable to Ambient Air Pollution: An Analysis of Data from the Global Burden of Diseases Study 2015. *Lancet* **2017**. https://doi.org/10.1016/S0140-6736(17)30505-6.

(47) Sun, G.; Crissman, K.; Norwood, J.; Richards, J.; Slade, R.; Hatch, G. E. Oxidative Interactions of Synthetic Lung Epithelial Lining Fluid with Metal-Containing Particulate Matter. *Am. J. Physiol. - Lung Cell. Mol. Physiol.* **2001**, *281* (4), L807 LP-L815.

(48) Wojas, B.; Almquist, C. Mass Concentrations and Metals Speciation of PM2.5, PM10, and Total Suspended Solids in Oxford, Ohio and Comparison with Those from Metropolitan Sites in the Greater Cincinnati Region. *Atmos. Environ.* **2007**, *41* (39), 9064–9078. https://doi.org/10.1016/j.atmosenv.2007.08.010.

(49) Boohene, M.; Sulemana, R.; SOSSOU, K. Assessment of Heavy Metal Concentrations in Particulate Matter (PM10) in the Ambient Air of Selected Roadsides in the Accra Metropolis of Ghana, West Africa. **2019**, *vol 6*, 34–54.

(50) Hama, S. M. L.; Cordell, R. L.; Staelens, J.; Mooibroek, D.; Monks, P. S. Chemical Composition and Source Identification of PM10 in Five North Western European Cities. *Atmos. Res.* **2018**, *214*, 135–149. https://doi.org/10.1016/j.atmosres.2018.07.014.

(51) Negral, L.; Suárez-Peña, B.; Zapico, E.; Fernández-Nava, Y.; Megido, L.; Moreno, J.; Marañón, E.; Castrillón, L. Anthropogenic and Meteorological Influences on PM10 Metal/Semi-Metal Concentrations: Implications for Human Health. *Chemosphere* **2020**, *243*, 125347. https://doi.org/10.1016/j.chemosphere.2019.125347.

(52) Maione, M.; Fowler, D.; Monks, P. S.; Reis, S.; Rudich, Y.; Williams, M. L.; Fuzzi, S. Air Quality and Climate Change: Designing New Win-Win Policies for Europe. *Environ. Sci. Policy* **2016**, *65*, 48–57. https://doi.org/http://dx.doi.org/10.1016/j.envsci.2016.03.011.

(53) Øvrevik, J.; Refsnes, M.; Låg, M.; Holme, J. A.; Schwarze, P. E. Activation of Proinflammatory Responses in Cells of the Airway Mucosa by Particulate Matter: Oxidant- and Non-Oxidant-Mediated Triggering Mechanisms. *Biomolecules* **2015**, *5* (3), 1399–1440. https://doi.org/10.3390/biom5031399.

(54) Pardo, M.; Shafer, M. M.; Rudich, A.; Schauer, J. J.; Rudich, Y. Single Exposure to near Roadway Particulate Matter Leads to Confined Inflammatory and Defense Responses: Possible Role of Metals. *Environ. Sci. Technol.* **2015**. https://doi.org/10.1021/acs.est.5b01449.

(55) Fang, T.; Guo, H.; Verma, V.; Peltier, R. E.; Weber, R. J. $PM_{2.5}$ Water-Soluble Elements in the Southeastern United States: Automated Analytical Method Development, Spatiotemporal Distributions, Source Apportionment, and Implications for Heath Studies. *Atmos. Chem. Phys.* **2015**, *15* (20), 11667–11682. https://doi.org/10.5194/acp-15-11667-2015.

(56) Weichenthal, S.; Shekarrizfard, M.; Kulka, R.; Lakey, P. S. J.; Al-Rijleh, K.; Anowar, S.; Shiraiwa, M.; Hatzopoulou, M. Spatial Variations in the Estimated Production of Reactive Oxygen Species in the Epithelial Lung Lining Fluid by Iron and Copper in Fine Particulate Air Pollution. *Environ. Epidemiol.* **2018**, *2* (3), e020. https://doi.org/10.1097/ee9.0000000000000020.

(57) Weichenthal, S.; Crouse, D. L.; Pinault, L.; Godri-Pollitt, K.; Lavigne, E.; Evans, G.; van Donkelaar, A.; Martin, R. V.; Burnett, R. T. Oxidative Burden of Fine Particulate Air Pollution and Risk of Cause-Specific Mortality in the Canadian Census Health and Environment Cohort (CanCHEC). *Environ. Res.* **2016**, *146*, 92–99. https://doi.org/10.1016/j.envres.2015.12.013.

(58) IARC. *Air Pollution and Cancer, IARC Publication No. 161*; Lyon, France, 2013.

(59) Bellinger, D.; Leviton, A.; Waternaux, C.; Needleman, H.; Rabinowitz, M. Longitudinal Analyses of Prenatal and Postnatal Lead Exposure and Early Cognitive Development. *N. Engl. J. Med.* **1987**, *316* (17), 1037–1043.

(60) Gottipolu, R. R.; Landa, E. R.; Schladweiler, M. C.; McGee, J. K.; Ledbetter, A. D.; Richards, J. H.; Wallenborn, G. J.; Kodavanti, U. P. Cardiopulmonary Responses of Intratracheally Instilled Tire Particles and Constituent Metal Components. *Inhal. Toxicol.* **2008**, *20* (5), 473–484. https://doi.org/10.1080/08958370701858427.

(61) Li, Q.; Liu, H.; Alattar, M.; Jiang, S.; Han, J.; Ma, Y.; Jiang, C. The Preferential Accumulation of Heavy Metals in Different Tissues Following Frequent Respiratory Exposure to PM2.5 in Rats. *Sci. Rep.* **2015**, *5*, 16936.

(62) Gibson, M. D.; Haelssig, J.; Pierce, J. R.; Parrington, M.; Franklin, J. E.; Hopper, J. T.; Li, Z.; Ward, T. J. A Comparison of Four Receptor Models Used to Quantify the Boreal Wildfire Smoke Contribution to Surface $PM_{2.5}$ in Halifax, Nova Scotia during the BORTAS-B Experiment. *Atmos. Chem. Phys.* **2015**, *15* (2), 815–827. https://doi.org/10.5194/acp-15-815-2015.

(63) Cohen, D. D.; Stelcer, E.; Hawas, O.; Garton, D. IBA Methods for Characterisation of Fine Particulate Atmospheric Pollution: A Local, Regional and Global Research Problem. *Nucl. Instruments Methods Phys. Res. Sect. B Beam Interact. with Mater. Atoms* **2004**, *219–220*, 145–152. https://doi.org/10.1016/j.nimb.2004.01.043.

(64) Betha, R.; Behera, S. N.; Balasubramanian, R. 2013 Southeast Asian Smoke Haze: Fractionation of Particulate-Bound Elements and Associated Health Risk. *Environ. Sci. Technol.* **2014**, *48* (8), 4327–4335. https://doi.org/10.1021/es405533d.

(65) Councell, T. B.; Duckenfield, K. U.; Landa, E. R.; Callender, E. Tire-Wear Particles as a Source of Zinc to the Environment. *Environ. Sci. Technol.* **2004**, *38* (15), 4206–4214. https://doi.org/10.1021/es034631f.

(66) Pacyna, J. M.; Pacyna, E. G. An Assessment of Global and Regional Emissions of Trace Metals to the Atmosphere from Anthropogenic Sources Worldwide. *Environ. Rev.* **2001**, *9* (4), 269–298. https://doi.org/10.1139/a01-012.

(67) Gibson, M. D.; Pierce, J. R.; Waugh, D.; Kuchta, J. S.; Chisholm, L.; Duck, T. J.; Hopper, J. T.; Beauchamp, S.; King, G. H.; Franklin, J. E.; et al. Identifying the Sources Driving Observed PM2.5 Temporal Variability over Halifax, Nova Scotia, during BORTAS-B. *Atmos. Chem. Phys.* **2013**, *13* (14), 7199–7213. https://doi.org/10.5194/acp-13-7199-2013.

(68) Wang, X.; Bi, X.; Sheng, G.; Fu, J. Chemical Composition and Sources of PM10 and PM2.5 Aerosols in Guangzhou, China. *Environ. Monit. Assess.* **2006**, *119* (1), 425–439. https://doi.org/10.1007/s10661-005-9034-3.

(69) Grigoratos, T.; Martini, G. Brake Wear Particle Emissions: A Review. *Environ. Sci. Pollut. Res.* **2015**, *22* (4), 2491–2504. https://doi.org/10.1007/s11356-014-3696-8.

(70) Wai, K.-M.; Wu, S.; Li, X.; Jaffe, D. A.; Perry, K. D. Global Atmospheric Transport and Source-Receptor Relationships for Arsenic. *Environ. Sci. Technol.* **2016**, *50* (7), 3714–3720. https://doi.org/10.1021/acs.est.5b05549.

(71) Rauch, J. N.; Pacyna, J. M. Earth's Global Ag, Al, Cr, Cu, Fe, Ni, Pb, and Zn Cycles. *Global Biogeochem. Cycles* **2009**, *23* (2), GB2001. https://doi.org/10.1029/2008GB003376.

(72) Herner, J. D.; Green, P. G.; Kleeman, M. J. Measuring the Trace Elemental Composition of Size-Resolved Airborne Particles. *Environ. Sci. Technol.* **2006**, *40* (6), 1925–1933. https://doi.org/10.1021/es052315q.

(73) EPA. National Ambient Air Quality Standards (NAAQS).

(74) IMPROVE. Reconstructing Light Extinction from Aerosol Measurements.

(75) USEPA. Chemical Speciation Network Database.

(76) Taylor, S. R.; McLennan, S. M. The Geochemical Evolution of the Continental Crust. *Rev. Geophys.* **1995**, *33* (2), 241–265. https://doi.org/10.1029/95RG00262.

(77) Hsu, S. C.; Liu, S. C.; Tsai, F.; Engling, G.; Lin, I. I.; Chou, C. K. C.; Kao, S. J.; Lung, S. C. C.; Chan, C. Y.; Lin, S. C.; et al. High Wintertime Particulate Matter Pollution over an Offshore Island (Kinmen) off Southeastern China: An Overview. *J. Geophys. Res. Atmos.* **2010**, *115* (D17), D17309. https://doi.org/10.1029/2009JD013641.

(78) Cesari, D.; Contini, D.; Genga, A.; Siciliano, M.; Elefante, C.; Baglivi, F.; Daniele, L. Analysis of Raw Soils and Their Re-Suspended PM10 Fractions: Characterisation of Source Profiles and Enrichment Factors. *Appl. Geochemistry* **2012**, *27* (6), 1238–1246. https://doi.org/10.1016/j.apgeochem.2012.02.029.

(79) Malm, W. C.; Hand, J. L. An Examination of the Physical and Optical Properties of Aerosols Collected in the IMPROVE Program. *Atmos. Environ.* **2007**, *41* (16), 3407–3427. https://doi.org/10.1016/j.atmosenv.2006.12.012.

(80) Malm, W. C.; Sisler, J. F.; Huffman, D.; Eldred, R. A.; Cahill, T. A. Spatial and Seasonal Trends in Particle Concentration and Optical Extinction in the United States. *J. Geophys. Res.* **1994**, *99* (D1), 1347–1370.

(81) Park, R. J.; Jacob, D. J.; Chin, M.; Martin, R. V. Sources of Carbonaceous Aerosols over the United States and Implications for Natural Visibility. *J. Geophys. Res. Atmos.* **2003**, *108* (12). https://doi.org/10.1029/2002jd003190.

(82) Behera, S. N.; Sharma, M. Reconstructing Primary and Secondary Components of PM2.5 Composition for an Urban Atmosphere. *Aerosol Sci. Technol.* **2010**, *44* (11), 983–992. https://doi.org/10.1080/02786826.2010.504245.

(83) Zhang, J.; Wu, Y.; Liu, C. L.; Shen, Z. B.; Zhang, Y. Major Components of Aerosols in North China: Desert Region and the Yellow Sea in the Spring and Summer of 1995 and 1996. *J. Atmos. Sci.* **2002**, *59* (9), 1515–1532. https://doi.org/10.1175/1520-0469(2002)059<1515:MCOAIN>2.0.CO;2.

(84) Das, R.; Khezri, B.; Srivastava, B.; Datta, S.; Sikdar, P. K.; Webster, R. D.; Wang, X. Trace Element Composition of PM2.5 and PM10 from Kolkata – a Heavily Polluted Indian Metropolis. *Atmos. Pollut. Res.* **2015**, *6* (5), 742–750. https://doi.org/http://dx.doi.org/10.5094/APR.2015.083.

(85) WHO, W. H. O. Air Quality Guidelines for Europe. **2000**.

(86) Okuda, T.; Kato, J.; Mori, J.; Tenmoku, M.; Suda, Y.; Tanaka, S.; He, K.; Ma, Y.; Yang, F.; Yu, X.; et al. Daily Concentrations of Trace Metals in Aerosols in Beijing, China, Determined by Using Inductively Coupled Plasma Mass Spectrometry Equipped with Laser Ablation Analysis, and Source Identification of Aerosols. *Sci. Total Environ.* **2004**, *330* (1–3), 145–158. https://doi.org/10.1016/j.scitotenv.2004.04.010.

(87) Pacyna, E. G.; Pacyna, J. M.; Fudala, J.; Strzelecka-Jastrzab, E.; Hlawiczka, S.; Panasiuk, D.; Nitter, S.; Pregger, T.; Pfeiffer, H.; Friedrich, R. Current and Future Emissions of Selected Heavy Metals to the Atmosphere from Anthropogenic Sources in Europe. *Atmos. Environ.* **2007**, *41* (38), 8557–8566. https://doi.org/10.1016/j.atmosenv.2007.07.040.

(88) Liu, G. J.; Zheng, L. G.; Duzgoren-Aydin, N. S.; Gao, L. F.; Liu, J. H.; Peng, Z. C. Health Effects of Arsenic, Fluorine, and Selenium from Indoor Burning of Chinese Coal. *Reviews of Environmental Contamination and Toxicology*. 2007, pp 89–106. https://doi.org/10.1007/978-0-387-35368-5_4.

(89) Duan, J.; Tan, J. Atmospheric Heavy Metals and Arsenic in China: Situation, Sources and Control Policies. *Atmos. Environ.* **2013**, *74*, 93–101. https://doi.org/http://dx.doi.org/10.1016/j.atmosenv.2013.03.031.

(90) Santoso, M.; Lestiani, D. D.; Kurniawati, S.; Markwitz, A.; Trompetter, W. J.; Barry, B.; Davy, P. K. Long Term Airborne Lead Pollution Monitoring in Bandung, Indonesia. *Int. J. PIXE* **2014**, *24* (03n04), 151–159. https://doi.org/10.1142/s0129083514400087.

(91) Zakiyya, H.; Distya, Y. D.; Ellen, R. A Review of Spent Lead-Acid Battery Recycling Technology in Indonesia: Comparison and Recommendation of Environment-Friendly Process. In *IOP Conference Series: Materials Science and Engineering*; Institute of Physics Publishing, 2018; Vol. 288. https://doi.org/10.1088/1757-899X/288/1/012074.

(92) Habibu, S.; Koki, I. B.; Tukur, A. I.; Gumel, S. M.; Ado, A.; Ladan, M.; Muhammad, A. A. A Reviewon Industrial Effluents as Major Sources of Water Pollution in Nigeria Riverbank Filtration and Surface Water Pollution View Project Electrochemical Sensor View Project A Review on Industrial Effluents as Major Sources of Water Pollution in Nigeria. *Chem. J.* **2015**, *1* (5), 159–164.

(93) Balasubramanian, R.; Qian, W. B. Characterization and Source Identification of Airborne Trace Metals in Singapore. *J. Environ. Monit.* **2004**, *6* (10), 813–818. https://doi.org/10.1039/b407523d.

(94) EMA. *Singapore Energy Statistics*; Singapore, 2017.

(95) Querol, X.; Alastuey, A.; Ruiz, C. R.; Artiñano, B.; Hansson, H. C.; Harrison, R. M.; Buringh, E.; Ten Brink, H. M.; Lutz, M.; Bruckmann, P.; et al. Speciation and Origin of PM10 and PM2.5 in Selected European Cities. *Atmos. Environ.* **2004**, *38* (38), 6547–6555. https://doi.org/10.1016/j.atmosenv.2004.08.037.

(96) Amato, F.; Alastuey, A.; Karanasiou, A.; Lucarelli, F. AIRUSE-LIFE+: A Harmonized PM Speciation and Source Apportionment in 5 Southern European Cities. *Artic. Atmos. Chem. Phys.* **2015**. https://doi.org/10.5194/acpd-15-23989-2015.

(97) Thomsen, V.; Schatzlein, D.; Mercuro, D. Limits of Detection in Spectroscopy. *Spectroscopy* **2003**, *18* (12), 112–114.

(98) Rahman, M. M.; Begum, B. A.; Hopke, P. K.; Nahar, K.; Thurston, G. D. Assessing the PM2.5 Impact of Biomass Combustion in Megacity Dhaka, Bangladesh. *Environ. Pollut.* **2020**, *264*, 114798. https://doi.org/10.1016/j.envpol.2020.114798.

(99) Zhang, Q.; Zheng, Y.; Tong, D.; Shao, M.; Wang, S.; Zhang, Y.; Xu, X.; Wang, J.; He, H.; Liu, W.; et al. Drivers of Improved PM2.5 Air Quality in China from 2013 to 2017. *Proc. Natl. Acad. Sci. U. S. A.* **2019**, *116* (49), 24463–24469. https://doi.org/10.1073/pnas.1907956116.

(100) Schlesinger, W. H.; Klein, E. M.; Vengosh, A.; Duce, R. A.; Friedland, A. J.; Galloway, J. N. Global Biogeochemical Cycle of Vanadium. **2017**. https://doi.org/10.1073/pnas.1715500114.

(101) Woo, M. K.; Young, E. S.; Mostofa, M. G.; Afroz, S.; Sharif Ibne Hasan, M. O.; Quamruzzaman, Q.; Bellinger, D. C.; Christiani, D. C.; Mazumdar, M. Lead in Air in Bangladesh: Exposure in a Rural Community with Elevated Blood Lead Concentrations among Young Children. *Int. J. Environ. Res. Public Health* **2018**, *15* (9). https://doi.org/10.3390/ijerph15091947.